Optimal Farm Design with Parabolic Shape Photovoltaic Panels Using Multi-objective Optimization

by

Zakiya Alfughi

A Thesis Submitted in Partial Fulfillment
of the Requirements for the Degree of

Master of Applied Science

in

Electrical and Computer Engineering

Department of Electrical, Computer, and Software Engineering

University of Ontario Institute of Technology (UOIT)

Oshawa, Ontario, Canada

April 2015

I hereby declare that I am the sole author of this thesis. This is a true copy of the thesis, including any required final revisions, as accepted by my examiners.
I understand that my thesis may be made electronically available to the public.

Zakiya Alfughi

Abstract

To acquire the maximum efficiency for solar electricity conversion, a solar panel has to absorb nearly every single photon of light emitted from the sun. The shape of the solar panel itself plays an important role in achieving this goal. Several studies have been conducted for different solar panel designs regardless of change in their internal or external shapes. In the first part of this thesis, a survey of solar photovoltaic (PV) panel shapes together with the advantages and disadvantages of the shapes is presented. The second part deals with using parabolic trough PV panels to obtain an optimal field design with two objectives, namely, maximum incident energy and minimum of the deployment cost. This design involves the relationships between the field and collector decision parameters and solar radiation data. In our proposed model, these parameters are the number of collector rows (K), the center-to-center distance between collectors (P), dimension of collectors (H), collectors inclination angle (β), and the rim angle of the collectors (ψ). Moreover, solar collectors arranged in rows in solar fields may be subjected to shading which depends on the spacing between the collector rows, the collector height, and the inclination angle, to some extent also on the row length and on the latitude of the solar field. The proposed mathematical model of PV panels is presented in details. A multi-objective evolutionary algorithm, called Non-dominated Sorting Genetic Algorithm-II (NSGA-II), is used to achieve the optimal field design with parabolic trough panels. Finally, the

performance of parabolic and flat panels are compared and the obtained results are discussed in detail.

Keywords: Photovoltaic, Parabolic Trough Panel, Multi-objective Optimization, NSGA-II, Solar Energy, Efficiency, Evolutionary Computation, Solar Farm.

Acknowledgements

I cannot find words to express my gratitude to my parents Mr. Gheit Alfughi and Mrs. Hawa Omer for their support and help during my whole life especially in my academic studies. Also, my sisters, and my brothers for encouraging me with their best wishes.

I would like to thank my small family, my husband, Khalid Addeeb and my lovely daughters. They were always cheering me up and stood by me through the good and bad times.

I would like to express my deep and sincere gratitude to my supervisor, Dr. Shahryar Rahnamayan and my co-supervisor, Dr. Bekir Yilbas, for their valuable guidance and never-ending support. Their enthusiasm has been the sources of inspiration and encouragement.

The financial support provided by the Libyan Ministry of Higher Education and Scientific Research is gratefully acknowledged.

Thanks to all of the teaching staff in Faculty of Engineering and Applied Science at UOIT University for their support and cooperation during the whole study period.

Contents

List of Figures

List of Tables

List of Acronyms

DE Differential evolution

PSO Particle swarm optimization

GAs Genetic algorithms

NSGA-II Non-dominated sorting genetic algorithm

EMO Evolutionary multi-objective optimization

MOP Multi-objective Optimization Problem

PVGCSs Photovoltaic grid-connected systems

CPC Compound parabolic concentrator

PTC Parabolic trough collector

PV Photovoltaic

Nomenclature

α	a field orientation angle defined as the angle made in the horizontal plane between horizontal line due south and projection of troughs focal line on horizontal plane; positive in anticlockwise direction (^{0})
β	collector inclination angle (^{0})
ΔT	time interval within which values of all the parameters are assumed to remain constant (s)
δ	declination angle (^{0})
γ	surface azimuth angle; due south is zero and positive in anticlockwise direction (^{0})
γ_s	solar azimuth angle; due south is zero and positive in anticlockwise direction (^{0})
$\mathbb{Z}^+$	natural number set
ω	hour angle; positive in morning, negative in afternoon and zero at solar noon (^{0})
ϕ	latitude (^{0})
ψ	rim angle, i.e. the angle between the optical axis and the line between the focal point and the mirror rim (^{0})
θ	angle between sun rays and aperture normal (^{0})
θ_z	zenith angle (^{0})
A_{max}	maximum collector height above ground
A_s	instantaneous shaded area (m^2)
a_s	instantaneous non-dimensional shaded area
E_{avl}	energy available on unit aperture area of trough after considering shading (J/m^2)

E_{inc} energy incident on unit aperture area of trough without considering shading (J/m^2)

f focal length, i.e. the distance between the focal point and the vertex of a parabola (m)

H collector height (m)

H_s instantaneous shaded height of a row (m)

h_s instantaneous non-dimensional shaded height of a row

I_{bn} instantaneous beam normal radiation (W/m^2)

I_d instantaneous diffuse radiation (W/m^2)

L length of each row (m)

L_s instantaneous shaded length of a row (m)

l_s instantaneous non-dimensional shaded length of a row

N number of intervals in which the time period

P pitch, i.e. perpendicular distance between two consecutive focal axes of troughs (m)

P_r price of single panel($)

Q yearly energy (J/m^2)

W solar field width (m)

T_R sun rise on the collector (s)

T_S sun set on the collector (s)

Chapter 1

Introduction

1.1 Motivation

The development of a precise, highly efficient, and economic solar farm has motivated many researchers to develop an optimal PV farm design to satisfy these issues. Several works were devoted to the optimal design of PV systems, mainly from the economic viewpoint. The majority of these works are conducted to minimize cost or maximize produced annual energy (i.e. mono-objective optimization problem). After that, solar collector field design formulated as a multi-objective optimization problem. Whether they used metaheuristic or mathematical approaches to solve the optimization problem, the PV system designs are still limited to the flat panels.

Studies [18], [19], [20] investigated the configuration setup of flat PV panels in order to harvest more energy with low cost. Recently, the work in [21] presented the optimal design of stationary multi-row compound parabolic concentrator (CPC) solar collectors. Therefore, using another PV shape is of interest.

Since parabolic trough collectors have been the commercially most successful technology used for solar thermal power plants, we proposed the using PV panels with parabolic trough shape. To the best of our knowledge, the proposed model in this thesis is the first attempt to optimize the configuration setup of PV panels with parabolic trough shape using optimizing multiple objectives.

1.2 Objectives and Scope

The work presented in this thesis has two objectives. First, conducting a review study of the existing photovoltaic shapes whether are internal or external. Furthermore, the pros and cons of these shapes are taken into account during the review. A comparison between the performance of these shapes and flat PVs performance is studied. The second objective is to achieve an optimal PV farm design which

yields maximum field incident energy with a minimum deployment cost. As the solar collector field design formulated as a multi-objective optimization problem, we applied constraints optimization techniques to solve it. A multi-objective evolutionary algorithm named Nondominated Sorting Genetic Algorithm-II (NSGA-II) used to achieve the optimal field design with parabolic trough panels. Then the performance of parabolic and flat panels is compared and the obtained results are discussed in detail.

1.3 Organization of the thesis

This thesis consists of seven chapters and one appendix which are organized as follows:

Chapter 2 presents a background on the parabolic trough collector and its geometries. It also discusses some solar angles which used in the thesis along with the definition of some solar related terms.

Chapter 3 is a survey of solar panel shapes together with the advantages and disadvantages of these shapes.

A brief introduction of multi-objective optimization and its concepts is provided in **Chapter 4**. Besides, non-dominated sorting genetic algorithm (NSGA-II) is explained as an example of multi-objective evolutionary algorithms used to achieve the optimal field design.

The core concept of this thesis is presented in **Chapter 5**. First, related works of using PV panels in PV farms are provided. Then, the modeling approach is discussed in detail.

The obtained results and discussion are presented in **Chapter 6**.

The conclusions, contributions, and future works all are addressed in **Chapter 7**.

Finally, **Appendix B** describes the meteorological data of Toronto, used in our optimal photovoltaic farm design.

Chapter 2

Background Review

This chapter aims to provide a description of the parabolic trough collector which is used in our model. Definitions of some terms related to this collector are presented in Section 2.1. In Section 2.2, some solar angles, which affect the absorbed energy of a panel and used in our model are defined in detail.

2.1 Parabolic trough collectors

This thesis specifically utilizes parabolic trough panels for converting sunlight into electricity. The parabolic curvature, as shown in Figure 2.1, is described by the formula $Z = \frac{x^2}{4f}$. The distance f represents the position of the focal point of the parabola, essentially the distance of the focal line of the parabola from its vertex. All radiation parallel to the axis of the parabola are reflected to the focal point f.

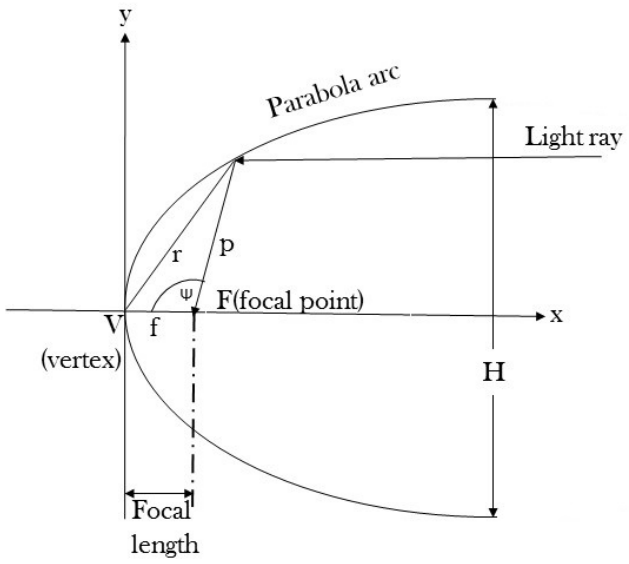

Figure 2.1: Cross section view of a parabolic collector, r is the distance from the origin, θ the angle from the x-axis to r, and p is the parabolic radius.

Different from flat panels which just height and length are needed to determine the shape of the panel; four parameters are required to determine the cross-section of

a parabolic trough completely, i.e. shape and size. These parameters are rim angle ψ, aperture width H, trough length l, and focal length f. The aperture width H can be expressed as a function of the rim angle and the focal length as follow [22]:

$$H = f \times \left(-\frac{4}{\tan(\psi)} + \sqrt{\frac{16}{\tan^2(\psi)} + 16} \right) \tag{2.1}$$

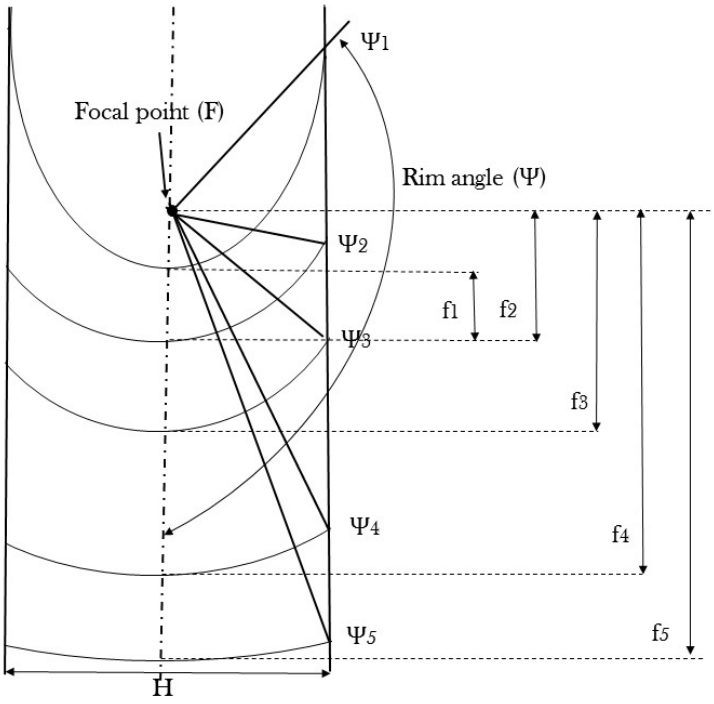

Figure 2.2: Relation between the focal length f and the rim angle ψ for a constant trough aperture width H.

The rim angle is considered as a very important constructive trait of collectors because it defines the shape of collectors' arc as shown in Figure 2.2. Consequently, it affects the efficiency of the collectors. With the same aperture width H, if the rim angle is very big, then the parabolic trough will be very narrow which prevents the Sun rays to hit the whole surface. And, if the rim angle is very small, then the collector is similar to a flat panel [23]. In this case, the surface area of the parabolic

trough will be decreased with the decreasing of the cross-section length of the trough. So, the rim angle should neither be too small nor too large.

The surface area or the aperture area of a parabolic trough is calculated

$$A = S \times L, \tag{2.2}$$

where S is the length of the parabola that is the cross-section of the trough. S can be calculated according to the following formula

$$S = \left(\frac{H}{2} \sqrt{1 + \frac{H^2}{16f^2}} + 2f \times log \left(\frac{H}{4f} + \sqrt{1 + \frac{H^2}{16f^2}} \right) \right) \tag{2.3}$$

2.2 Solar Time and Solar Angles

The absorbed solar energy of a surface is affected by the angle at which the incoming solar beam radiation hits that surface. The angle of incidence, θ, is an angle between a normal to the collector face and the incoming solar beam. It depends on the latitude ϕ, hour solar angle ω, and declination angle δ. These three angles describe the position of the sun for its daily path and will be explained herein. Furthermore, Table 2.1 summarizes some solar angles. All the equations used in this section are according to [17].

$$\cos\theta = \cos\delta \left[\sin^2\omega + (\cos\phi\cos\omega - \tan\delta\sin\phi)^2 \right]^{\frac{1}{2}} \tag{2.4}$$

The declination, δ (Figure 2.4), is the angular position of the sun at solar noon (i.e., when the sun is on the local meridian) with respect to the plane of the equator. It reaches its minimum of -23.45^0 at the winter solstice (22 December) and its maximum of 23.45^0 at the summer solstice (21 June). The angle is zero at the vernal equinox

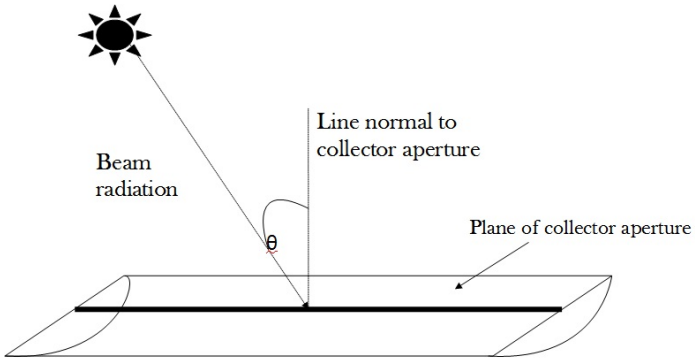

Figure 2.3: Incidence angle θ.

(22 March) and at the autumnal equinox (23 September). The occurrence of solar declination angle at any moment in the annual motion is strictly known. Several expressions giving the approximate value of solar declination have been suggested. A further and simple equation is given as follow (Cooper, as quoted in [17]):

$$\delta = 23.45 \sin(360(\frac{284+n}{365})), \tag{2.5}$$

where n = day of the year

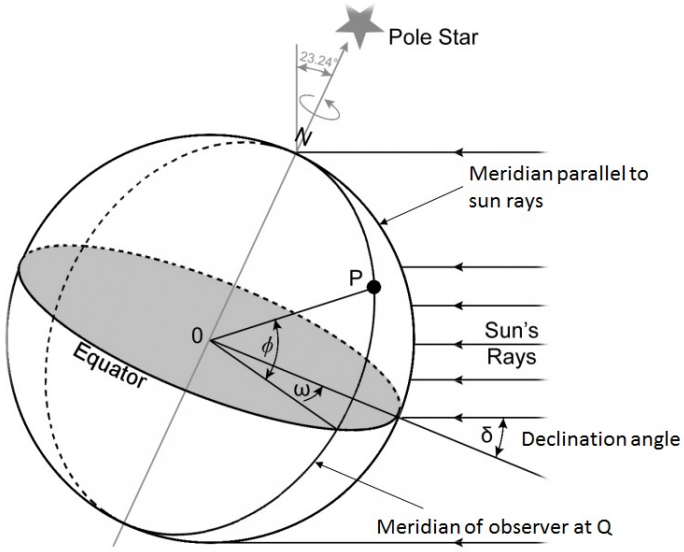

Figure 2.4: The declination angle (δ), latitude (ϕ) and the hour angle (ω) for point P.

The hour angle, ω , as shown in Figure 2.4, is the angular distance between the meridian of the observer and the meridian whose plane contains the sun. It is zero when the sun reaches its highest point in the sky (solar noon). At this time the sun is said to be due south (or due north, in the Southern Hemisphere) since the meridian plane of the observer contains the sun. The hour angle increases by 15 degrees every hour according to the Earth rotation and can be determined by Equation 2.6.

$$\omega = (Solartime - 12) \times 15 \tag{2.6}$$

The solar time, time defined by the position of the sun and is used in all the sun-angle relationships. It differs from the local clock time based on Equation 2.7

$$\begin{aligned} solartime = standardtime + 4(\mathrm{L}_{ST} \text{ - } L_{LOC}\ ) \\ +\mathrm{EOT} \end{aligned} \tag{2.7}$$

The standard time is that of the local time zone. The standard meridian of the local time zone is represented by L_{ST}; whereas, L_{LOC} is the longitude of the exact location under consideration. The difference (L_{ST} - L_{LOC}) is multiplied by 4, the time (in minutes) required for the sun to move one radial degree across the sky. EOT represents the Equation of Time, which accounts for disturbances to the Earths rate of rotation, and can be calculated in minutes as follow

$$\begin{aligned} EOT = 229.2 \times (0.000075 + 0.001868\cos B - 0.032077\sin B \\ -0.014615\cos(2B) - 0.04089\sin(2B)), \end{aligned} \tag{2.8}$$

where

$$B = (n-1)\,\frac{360}{365} \tag{2.9}$$

where n = day of the year.

2.3 Summary

As mentioned in this chapter, the values of solar angles affect the amount of the received energy by a panel's surface. In fact, the shape of that panel plays very important role on the efficiency of the panel itself. The next chapter will be conducted a review of different PV shapes along with the advantages and disadvantages of these shapes. Furthermore, the efficiency improvements of the shapes will be reported.

Table 2.1: Solar Angles as Presented by Duffie and Beckman [17]

Solar Angle	**Symbol**	**Range**	**Description**
Latitude	ϕ	$-90^0 \leq \phi \leq 90^0$	Angular location North/-South of Equator (North positive)
Declination	δ	$-23.45^0 \leq \delta \leq 23.45^0$	Angular position of the sun at solar noon with respect to the plane of the equator (North positive)
Slope	β	$0^0 \leq \beta \leq 180^0$	Angle between plane of surface and the horizontal plane
Surface Azimuth Angle	γ	$-180^0 \leq \gamma \leq 180^0$	Deviation of the projection on a horizontal plane of the normal to the surface from the local meridian, with zero due South (East negative, West positive)
Solar Azimuth Angle	γ_s	$-180^0 \leq \gamma_s \leq 180^0$	Deviation of the projection on a horizontal plane of the line of sight to the sun from the local meridian, with zero due South (East negative, West positive)
Hour Angle	ω	$-180^0 \leq \omega \leq 180^0$	Angular displacement of the sun East or West of the local meridian due to the rotation of the Earth on its axis (before solar noon= negative, after solar noon = positive)
Incident Angle	θ	$0^0 \leq \theta \leq 90^0$	Angle between beam radiation on a surface and the normal to that surface
Zenith Angle	θ_z	$0^0 \leq \theta_z \leq 90^0$	Angle subtended by a vertical line to the zenith (point directly overhead) and the line of sight to the sun

Chapter 3

Optimal Photovoltaic Design: A Survey

In this chapter, a brief introduction to PV cell generations is provided in Section 3.2. These PV cell generation are classified based on the conversion efficiencies ratio of each of them. The survey of PV modification techniques is presented in Section 3.3. Four categories are considered which are development of the front cover of PV modules, improvement of the external shape of PV, modifying the internal PV shape, and adjusting the shape of PV cell concentrator.

3.1 Introduction

Solar energy is the light that comes from the sun and is the earth's most abundant energy source. Each day, more solar energy falls to the earth than the total amount of energy the planet's 5.9 billion inhabitants would consume in 27 years [24]. Solar energy is considered as an excellent alternative for fossil fuels like coal and petroleum because it is practically emission free while generating electricity. With solar energy the danger of further damage to the environment is minimized, and its generation of electricity produces no noise or any kind of pollution. On the other hand, there are several drawbacks, which are subject to changing output efficiencies based on external factors such as shade, cloudy weather, and covered by sands. The two major active solar technologies that convert sunlight into electricity are solar thermal plants and photovoltaic panels. Solar thermal plants or concentrating solar power such as trough solar technology indirectly generate electricity; but they are considered the most proven and lowest cost large-scale solar power technology [19]. Photovoltaic devices or solar cells are the most widely used technology which converts sunlight directly into electricity. Rapid growth of the PV market was started in the 1980s owing to the application of multi-megawatt PV plants for power generation. Similar to the telecommunication and computer sectors, the PV market is growing by 30-40%

each year [25]. Photovoltaic panel efficiency is defined as the ratio of output power to input power from the sunlight, i.e., the percentage of light energy that hits the panel is converted into electricity. The higher the efficiency, the more electricity is generated in a given space. Up to now, the energy conversion efficiency of commercial solar PV is limited by 15-19% [26]. However, solar cell efficiency is not equal to the panel efficiency. The panel efficiency is usually 1 to 3 % lower than the solar cell efficiency due to some circumstances such as glass reflection, frame shadowing, and atmospheric conditions, including direct solar radiation, air pollution, and cloud movements. Furthermore, the performance of a PV panel is also affected by its orientation and its tilt angle with the horizontal plane. These two parameters could change the amount of solar energy received by the surface of the PV panel. Most importantly, the shape of the solar panel whether is internal or external also affects the solar panel performance.

3.2 PV cell generations

Photovoltaic cells are classified into three generations. First generation technologies involve high energy and labour inputs which prevent any significant progress in reducing production costs. The first generation PV cells are typically made using silicon wafers. They can reach a theoretical limiting efficiency of 33%, and achieve an energy payback period of 1-2 years. At present, there is concurrent research into all of these generations, while first generation technologies are the most highly represented in commercial production. Second generation photovoltaic materials are based on the use of thin-film deposits of semiconductors. Typically, the efficiencies of thin-film solar cells (19.4%) are lower than the first generation solar cells, but manufacturing costs are also lower. The most successful second generation materials have been

cadmium telluride (CdTe), copper indium gallium selenide, amorphous silicon, and micromorphous silicon. Third generation technologies are defined as semiconductor devices. They aim to improve the poor electrical performance of second generation (thin-film technologies), while maintaining very low production costs. Current research is targeting conversion efficiencies of 30-60% while retaining low cost materials and manufacturing techniques. This generation includes approaches such as dye-sensitized solar cells, quantum dots, nano-antennaes, nanomodified materials, and organic cells [27].

3.3 PV modification

In the last few decades, there have been a number of studies on modification the shape of photovoltaic panels in order to enhance efficiency. In this section, we will divide these studies into the following categories.

3.3.1 Development of the front cover of PV modules

Photovoltaic modules are usually covered by a flat-parallel layer of glass. The cover is designed to protect the photocell from the inclemency of the weather, or particles of dust. On the other hand, the cover introduces losses due to two main factors: (1) reflection losses in the two interfaces of the cover and (2) losses due to light absorption when the light is travelling through the glass of the cover. Often an antireflection coating is added to the cell surface at extra cost, to reduce the reflection problem further. A potentially much lower cost alternative is to add geometrical features on the cell surface.

Scheydecker et al. [1] and Blieske et al. [28] considered the possibility of adding a structured surface to the cover, which acts to minimize reflection losses by redirect-

ing as much of the incident energy as possible into the PV module. In the early work reported [1], as shown in Figure 3.1, a grooved, prism-shaped structure is proposed. Such a structured transparent cover is mounted with the grooves pointing in a north south direction. It is most effective when the solar cell module tilted toward the north south on a rooftop; for instance, rainwater can run down the grooves, cleaning them effectively. The structure is of the arbitrary but macroscopic scale so that geometric optics are valid. This ensures (ignoring dispersion effects) independence from the wavelength. Using a ray-tracing procedure, Scheydecker et al.[1] calculated the transmission of the structured surface depending on the angle of incidence of incoming light rays. Furthermore, outdoor measurements were performed with two, almost identical, pyramidal textured, monocrystalline silicon solar cells. One of them was covered with a smooth glass plate, whereas the other was covered with the structured acrylic glass. Scheydecker et al. concluded that only a combination of structured cover and structured solar cell surface leads to high transmission values because large angles are likely to occur inside the structured cover. Pyramidal textured solar cells yield the best results. From the calculated 97.8% entering the structured glass cover, a measured 93.2% can be coupled into a pyramidal textured monocrystalline solar cell, with an improvement of 17% compared to a smooth, uncoated solar cell with a smooth glass cover. Outdoor measurements showed that a textured solar cell with a structured cover has between 5% and 10% higher values of short-circuit current than a textured cell with a smooth cover.

As opposed to Scheydecker et al. [1], Blieske et al. [28] focused on the optical modelling of pyramids instead of grooves and on experimental results with a real glass cover instead of a polymer cover. An optical simulation software, which is working on Monte Carlo ray-tracing, has been used. This software is used to study the effect of a texture in three dimensions and to determine the surface texture that allows

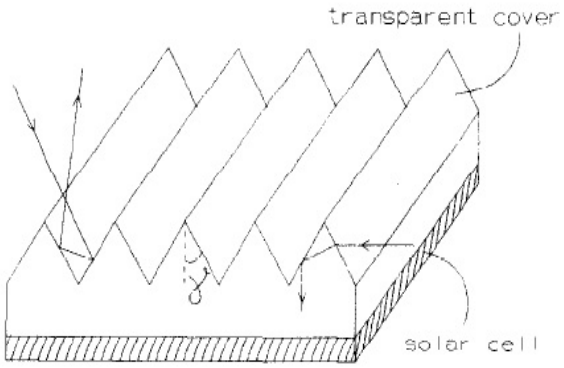

Figure 3.1: Grooved structure on a transparent cover of a solar cell. Reproduced from [1], Copyright (1994), with permission from Elsevier

the highest module performance. For each different geometry, the light transmission through the glass to the silicon solar cell as a function of the angle of incidence has been calculated and compared to the light transmission through a glass with a flat surface. Compared to a flat glass with the same composition, a front cover textured with inverse and positive pyramids (half-angle 45^0) allows to reduce reflection and enhance light trapping in standard solar modules. Moreover, the annual gain in efficiency is more than 6% for ideal structures. For real structures produced in industrial cast glass production in extra-white glass, the annual efficiency increase has been measured to be 3%. The previous covers could produce a small increase of the final cost of the solar panel because more sophisticated material and technology are needed to manufacture it.

Campbell et al. [29] defined a method for controlling the reflection in solar cells by adding geometrical features (pyramids and grooves) on the cell surface. Reduction of the reflection occurs by giving the light two chances of being coupled into the cell. A simply implemented approach, based on tilting these geometrical features, was used to show the performance of the solar cell. Computer ray tracing techniques were used to calculate the results of all such effects. The results show a reduction in the reflection from the cell surface, from 3-4% without antireflection coatings, to below

0.2%. Tilting of the geometrical features also allows very effective light trapping within the cell when combined with a planar rear surface. The improved reflection properties are relevant to all cells which use texturing, regardless of their design.

Illescas et al. [2] analyzed the light transmission properties of different structured-surface covers as compared to the standard flat-parallel model to elucidate the degree of improvement of these structures. As shown in Figure 3.2, an abrupt-shaped pattern of triangular form and a smoothed-shaped pattern of sinusoidal form were used. To accomplish the numerical calculations, Illescas et al. developed a novel optical simulation software application based on the widely used ray tracing technique. They chose to develop a new application instead of using existing optical simulators because of the following reasons:

- Some of these simulators are not easy to use due to the large amount of data needed to model any optical object and/or their wide range of available actions.
- Some do not offer a useful (or easy to manipulate) output for further processing of the data and/or do not offer a convenient energy analysis.

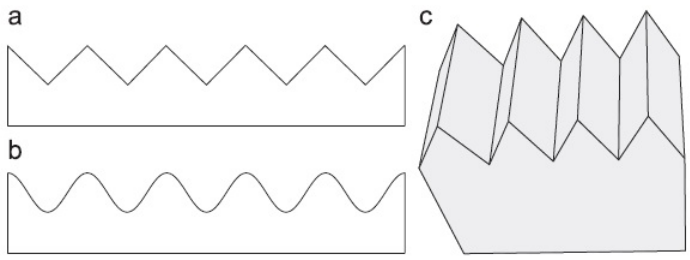

Figure 3.2: Schemes of the two geometries considered for the structured surfaces. Cases (a) and (b) correspond, respectively, to the side view of the triangle and the cosine geometry. Case (c) corresponds to a 3D top view of the triangle geometry. Reproduced from [2], Copyright (2008), with permission from Elsevier.

Regarding a comparison between pyramidal (an abrupt-shaped pattern) and sinusoidal (a smoothed-shaped pattern), there is no significant differences. PV modules with a fixed orientation can transmit from 35% to 55% more energy if they use

a structured cover with a pyramidal or sinusoidal pattern having $\theta \geq 40^0$ rather than a flat cover with a large incidence angle $\theta \geq 60^0$. These structures are also useful at normal incidence if the absorption is very small.

3.3.2 Improvement of the external shape of PV

From the time of the invention of silicon solar cells in 1954 [25], almost all kinds of solar cells have been designed to harvest sunlight with a flat panel. Since solar elevation and azimuth angles change continuously throughout the day, if there is no solar tracker, the decrease in energy production for solar cells roughly follows a cosine function. This happens because solar irradiance is not normal to the solar-cell surface during most time of the day. With the new PV technologies from second and third generation, the PV module is no longer flat; it can be moulded to any desired shape and geometry based on the application.

Myers et al. [3] combined a generic algorithm GA method and a code in order to obtain optimal 3D-PV shapes. They used the code to compute the energy generated in one day by an arbitrary shaped 3D solar cell. The solar power-collecting structures are defined as configurations of triangles in Cartesian space confined to a rectangular box volume whose face normals point North, South, East, and West. The triangles represent double-sided flat panel solar cells, and within the GA are allowed to evolve their coordinates independently to produce an optimized 3D structure. In the GA, candidate 3D structures are combined using operations based on the three principles of natural selection; selection, recombination, and mutation. Selection determines which structures will propagate to the next step, where they are modified by the recombination and mutation operators. The authors compared the energy generated by simple open-box shapes and the funnel structures as the ratio of the energy produced in a day to the total area of active material used, and scaled the result for the flat

panel case.

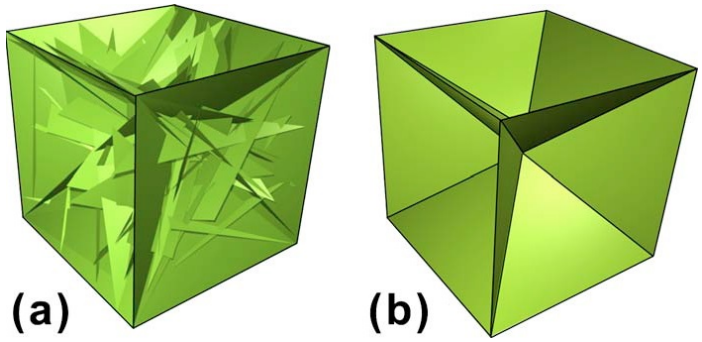

Figure 3.3: Schematics of 3D-PV structures: (a) GA-optimized structure shown with all 64 triangles inside the bounding box; (b) funnel, a simplified version of most GA-optimized structures that retains their superior performance over other shapes. Reproduced from [3], Copyright (2010), with permission from AIP Publishing LLC.

As a result of their experiment, Myers et al. concluded that there is an increase in power with height in the early morning and late afternoon, in contrast to the power generated by a flat panel, which, without dual-axis tracking, rapidly decays around peak-time. Optimal shapes resultant using a genetic algorithm approach included a cubic box open at the top and a cubic box with funnel-like shaped faces, both capable in principle of doubling the daily energy density. Furthermore, a 3D architecture as shown in Figure 3.3 could be optimized to capture light using multiple reflections while preventing shading of the active material, possibly limiting the need for expensive antireflective coatings. In addition, shapes that are optimized using a GA approach may allow for significant material saving and also the use of materials, within a wide reflectance range without affecting device performance.

Bernardi et al. [4], [30] demonstrated that 3D-PV structures that proposed in [3] can be realized practically and can dramatically improve solar energy generation. In order to experimentally study 3D-PV systems, Bernardi and his group fabricated and tested simple 3D-PV structures (Figure 3.4) consisting of a cube open at the top covered by solar cells both on the interior and exterior surfaces (an open cube

structure), a similar open parallelepiped of the same base area but twice as high, and a tower with ridged faces. In addition to the experimentally study, a simulation has also been done.

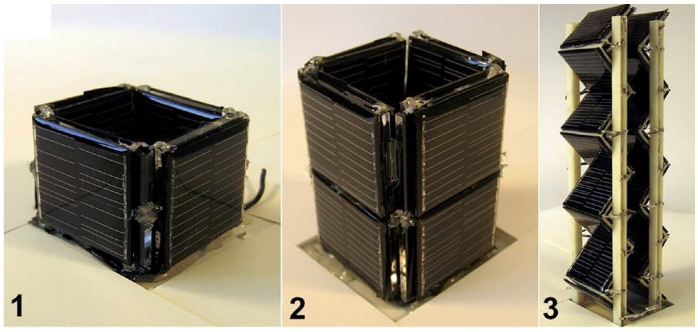

Figure 3.4: 3DPV structures: (1) an open cube , (2) an open parallelepiped twice as tall , and (3) a tower. The structures are made up, respectively, of 9, 17, and 32 solar cells. Reproduced from [4], Copyright (2012), with permission from Royal Society of Chemistry.

The generated energy can be expressed as an objective function of the cell coordinates and can thus be maximized using standard Monte Carlo (MC) simulated annealing and genetic algorithm (GA) optimization techniques. The performance of the 3D-PV was then measured under different weather conditions during different daylight hours. The authors concluded that an increase in the energy density by a factor of 2×20 in the absence of sun tracking was measured for the three fabrication structures. Moreover, they showed that using 3D-PV can double the peak power generation hours and reduce seasonal and latitude variability in the energy generation compared to flat panel design. More importantly, Bernardi et al. demonstrate that even though the area of PV material per unit of generated energy compared to flat panels is higher in the case of 3DPV, the module is no longer the main cost in PV installations and will continue to decrease relative to other costs.

Karavadi and Balog [5] presented a modeling approach and analysis to calculate the total amount of energy that is being captured by various non-flat PV surfaces throughout a day. A systematic comparison among these surfaces themselves, as

well as between flat PV surfaces, is provided to investigate which surface is better in harvesting energy. Furthermore, the modeling approach determines the view factors for each surface so that the amount of energy captured by various surface geometries can be studied. A three dimensional surface as shown in Figure 3.5 is created in MATLAB to represent the PV panel and to represent the various solar meshed cells.

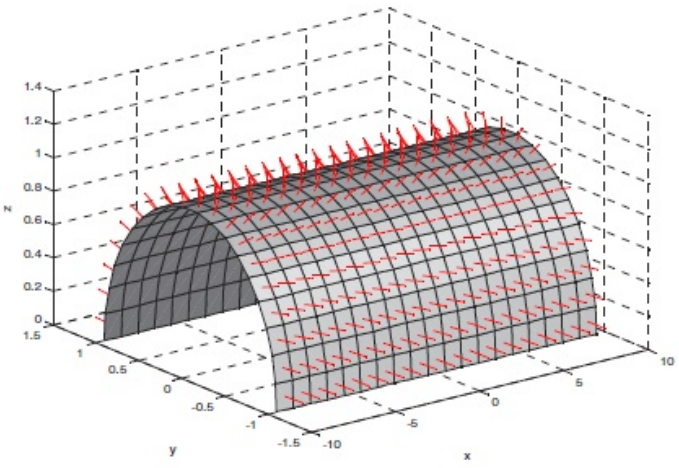

Figure 3.5: Semi cylinder with surface normals [5]. Copyright ©2011, IEEE.

Normal vectors are created for each cell and a line is drawn in the middle of these cells to showcase the various angles at which these are oriented considering that the sun is at one point in the sky. The location of the sun at any time of the day is described in terms of its altitude or elevation angle and its azimuth angle which depend on the latitude, day number and, most importantly, time of day. Moreover, the view factor is considered as the ratio of projected area of the surface and actual area of the surface, and can take values in the closed set of real numbers [0, 1]. Karavadi and Balog observed that, for a semi cylindrical and a cylindrical surface, the total amount of energy harvested in a particular day is more than a flat plate with 20.88% and 41.63%, respectively, when common latitude of 23.5^0 north is taken for comparison. Hemi sphere surface harvests more energy during early morning and

evening hours than a flat plate. However, the actual advantage of it can only be seen when the view factor of this surface is observed in the North Pole area.

Hiraki et al. [31] conducted a comparative study between a cylindrical PV module and a conventional CIGS (Copper Indium Gallium Selenide) PV module. Both modules were installed on a flat rooftop at an inclination of 0^0. Furthermore, a wind tunnel test was done in Okinawa in order to prove the reliability of self-ballasted installation. The authors installed cylindrical PV panels when typhoon No. 9 (in 2011) struck Okinawa and checked whether the panels had moved or not. In addition, a new concept of a combination of PV generation and agriculture is suggested by using cylindrical PV panels that do not fully shut out the sunlight, wind and rain which are needed for plant growth. By using this concept dual functions can be produced, first by using sunlight, which harvests crops and second function by converting sunlight into electricity. A small test field in the city of Aioi, Hyogo Prefecture, was completed to test this concept.

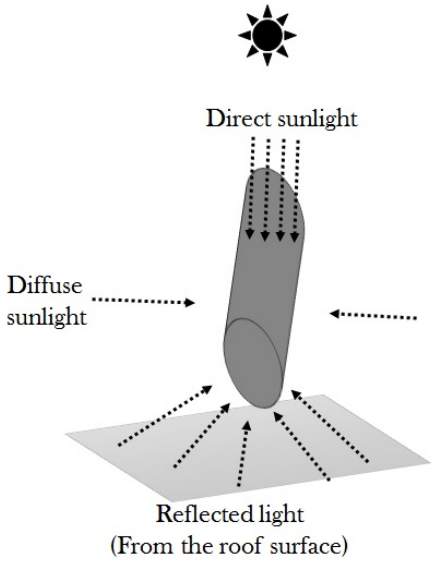

Figure 3.6: Collection of sunlight with cylindrical PV panel.

Hiraki et al. demonstrated that the cylindrical PV module captures sunlight

from an angular range of 360^0 (Figure 3.6) with a strong spectral absorption about 95% of the nominal power, which is 1 kW. Cylindrical PV modules also have functions of self-tracking and can capture more light early and late in the day. This means it can generate higher electric power than the conventional CIGS PV module. For the reliability of Self-ballasting, the panels had not moved at all, even though the maximum instantaneous wind speed of typhoon No. 9 was around 50 m/s. Finally, they have harvested some crops and generated electric power, as a new application of cylindrical PV in agricultural fields.

Sugathan et al. [6] proposed the development of a triangular prism shaped solar photovoltaic unit in order to reduce the required area for installation of the panels as opposed to the conventional method where the flat plate photovoltaic concept is used. The proposed model as shown in Figure 3.7 used three similar panels arranged in the form of a triangular prism. The prism is positioned in such a way, that one of its panels called the primary panel will be facing the sun, while the other two secondary panels does not face sun directly. Overall efficiency of the proposed system is improved by approximately 0.5%.

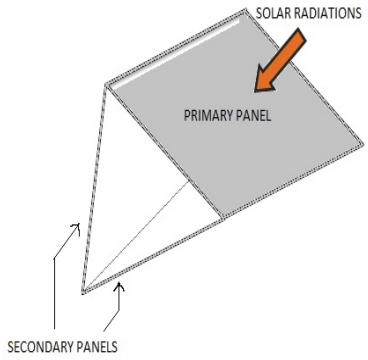

Figure 3.7: Triangular prism arrangement of panels [6]. Copyright ©2013, IEEE.

3.3.3 Modifying the internal PV shape

Alternative solar cell geometries have been proposed to resolve the problems in the flat solar cell design, such as reducing the conversion efficiency due to the presence of a non-transparent conducting grid on the electrode facing the incident light.

Yong et al. [32] proposed a novel solar cell fabricated by spiral photo-electrode for capturing sunlight from 3-dimensional space. This 3D-cell shows the same characteristics with needle leaves to receive sunlight. Compared with flat panel solar cells, a 3D-cell could track the sun passively to receive solar irradiance without cosine losses. To measure the performance of the cells, indoor measurements were conducted by a solar simulator (Orial, 100 W/cm^2). In this case, the 3D-cell was put vertically to receive simulated light. Secondly, because merits of the 3D-cell could not be evaluated by the traditional solar simulator, its performance in nature sunlight was also studied. All outside measurements were completed on the roof of Nano Center building in Sun Yat-sen University. Absorption spectra of samples were analyzed by a UV-Visible-NIR spectrophotometer (HITACHI, U-4100), and irradiance was measured by the pyranometer (SOLARWATT 98). In this case, the sun elevation angle was calculated to be 66.73^0 at noon on September 23 in Guangzhou. The cell was placed towards the south with a 23^0 incline to obtain direct sunlight perpendicularly at noon. For indoor measurement, the obtained efficiency was about 2.14%, whereas it was about 2.63% for outdoor measurement. In addition, the flank area of the 3D-cell for capturing diffuse and reflected light was 3.14 times larger than flat panel solar cells with the same projection area because a spiral photo-electrode can receive sunlight from all directions and therefore can track the sun passively. This solves the problem of cosine losses and increases the area to obtain the diffuse and reflected sunlight. Furthermore, it is much more insensitive to sun azimuth angle and shade. As a result, power generation will also increase.

In another effort to enhance the efficiency of solar panels, Liu et al. [7] proposed unique coral-shaped nanomaterials that can be made from porous materials such as tin oxide. However, changing the structure and morphology of the materials is difficult using current preparation methods. Liu et al. as shown in Figure 3.8 developed tin oxide nanomaterials shaped like corals, via a swallowing growth mechanism, which increases the surface area of cells, thereby increasing the efficiency of dye-sensitized solar cells compared with spherical shaped nanoparticles. The significant role of the radial coral-like structure is demonstrated as providing a larger effective surface area for dye adsorption, light absorption and utilization than for a spherical structure. The above prototypes [32], [7] involved a more complex cell design, which complicates cell fabrication. Tachan et al. [8] fabricated a dye-sensitized solar cell (DSSC) inside a glass tube to form a dye-sensitized solar tube (DSST). DSSTs as shown in Figure 3.9 have a number of intrinsic advantages over conventional flat DSSCs. A current collector can be mounted on the bottom inside the tube, which is a significant advantage over the flat system, where the current collector is mounted on the electrode facing the incident light. The latter reduces the conversion efficiency due to shading and limits the width and subsequently the length of the current collector grid lines. In contrast, in DSSTs the collector line can be relatively thick/wide because it is located in a place where at best diffuse light is entering the cell, thus keeping light losses small. Another advantage of the tube panel design is that incident light, approaching the surface under an angle, can be efficiently collected with horizontally mounted tube arrays; for instance, on flat rooftops.

Tachan et al. observed that a dye-sensitized solar tube produced a light-to-electric power conversion efficiency of 2.8%. Furthermore, shading of neighbouring tubes is avoided by keeping a distance in between, providing a simple installation. In addition, the tube geometry allows the use of current collectors without loss of the

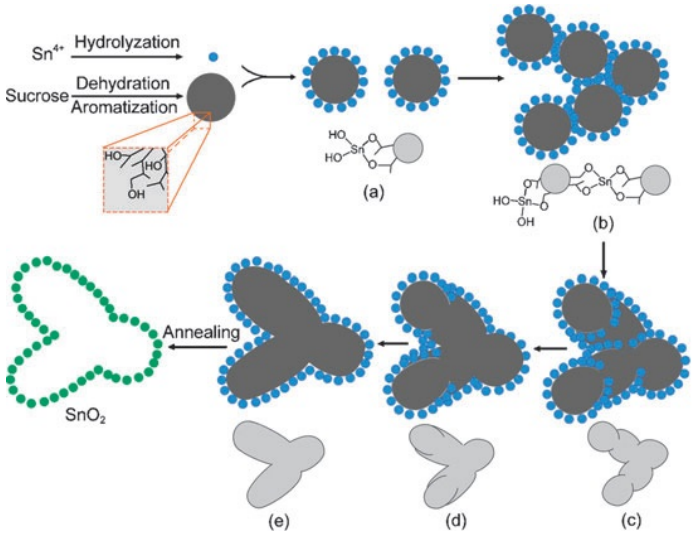

Figure 3.8: Schematic illustration of the proposed biomimetic swallowing formation process of coral-like porous SnO2 hollow architectures. Reproduced from [7], Copyright (2010), with permission from Royal Society of Chemistry

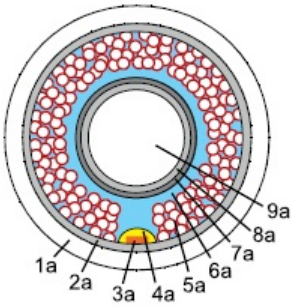

Figure 3.9: Schematic cross-section of a dye-sensitized solar tube(DSST)showing the glass tube (1a),the FTO layer deposited by spray pyrolysis (2a), a highly conducting current collector attached to the FTO on the bottom side inside the DSST (3a) and a polymer layer, which is protecting the current collector (4a). The mesoporous dye-sensitized TiO2 film (5a) deposited on to the FTO is immersed in to the redox electrolyte(6a).The circuit is closed by a counter electrode consisting of a sputtered Pt layer (7a) on top of a sprayed FTO film (8a), deposited on to a quartz rod (9a). Reproduced from [8], Copyright (2010), with permission from Elsevier.

active solar cell area that is exposed to direct sunlight.

Ning et al. [9] designed and synthesized a new kind of cone-shaped sensitizer by linking several long alkyl chains in the middle of the triarylamine-truexene based dyes (Figure 3.10). These sensitizers are used for dye-sensitized solar cells (DSSCs). A compact sensitizer layer is molecularly, interfacially engineered on the TiO_2 surface

of the DSSCs via cone-shaped sensitizers. As a result, the approach of the electrolyte to the TiO_2 surface is significantly blocked by the compact sensitizer layer formed, and the charge recombination in the DSSCs is proved to be effectively retarded. The monochromatic incident photon-to-current conversion efficiency of these sensitizers is almost 90%. Finally, the authors demonstrated that organic sensitizers are promising for the further improvement of the conversion efficiency of DSSCs.

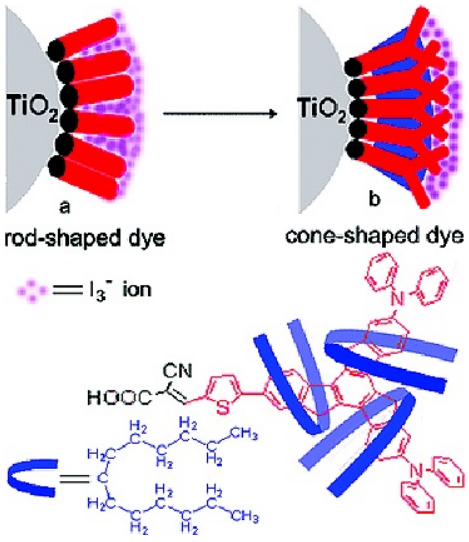

Figure 3.10: The simple sketch map of the cone-shaped sensitizer and the TiO_2 surface adsorbed with dye in the presence of redox electrolyte [9].

3.3.4 Adjusting the shape of PV cell concentrator

The use of solar concentrators has been proved as a feasible and low cost way to improve the cell's efficiency by condensing light illumination on the cells' surface.

Wenham et al. [10] as shown in Figure 3.11 modified the wedge-shaped concentrator by placing an identical concentrator on the other side of the cell and by replacing the rear surface mirror with a tilted groove structure. They used ray tracing for optimization of the module design. For a material with a refractive index of 1.5, the optimum side angle for the grooves was found to be 30^0 and the optimum

tilt angle of the module back surface was found to be 22^0. A three dimensional rear reflector ensured high collection efficiency of 15% with a high concentration ratio of 3.6:1, while simultaneously satisfying the dimensional constraints of standard roof tiles.

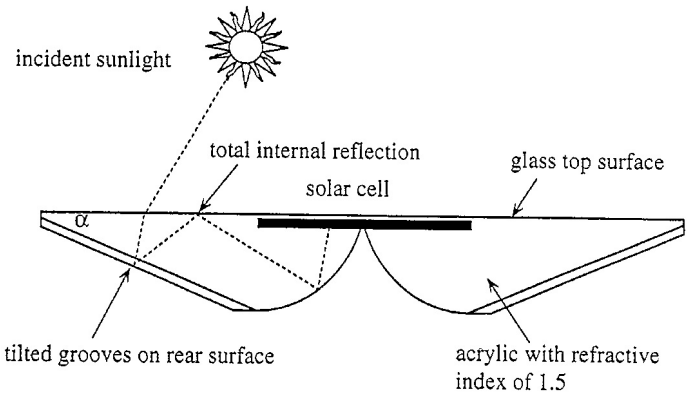

Figure 3.11: Static concentrator. Tilted rooves on the rear surface of the module run from the curved section to the edge. Reproduced from[10], Copyright (1997), with permission from Elsevier .

Maruyama and Osako [11] showed (Figure 3.12) a design method for the wedge-shaped concentrator without grooves, as opposed to [10]. Moreover, one- and two-stage concentrations, using the wedge-shaped concentrators, were discussed. A truncated-cone-shaped concentrator is also described as a modified three-dimensional wedge-shaped concentrator. Two-stage concentration can achieve a higher concentration ratio than one-stage concentration. For each value of the refractive index of the secondary concentrator, there is an optimum value of the refractive index for the primary concentrator which yields the maximum value of the overall concentration ratio. With a tracking system, a three-dimensional wedge-shaped concentrator can give higher concentration ratios than two-dimensional wedge-shaped concentrators. They found the orientation of the surface with incident light was very important.

Hughes et al. [12] investigated and compared the performance of realistically sized planar and a wedge-shaped luminescent solar concentrator (LSC) under direct

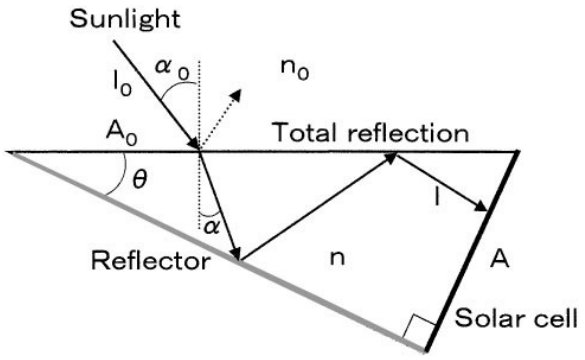

Figure 3.12: Wedge-shaped concentrator. Reproduced from [11], Copyright (1999), with permission from Elsevier.

illumination and to determine how their performance is affected by position of the sun. As opposed to the other wedge-shaped concentrators which used with PV cells, these incorporated fluorescent dyes. In addition, different orientations of the PV cell with bottom and top surface were used. As shown in Figure 3.13 the light moving towards the solar cells strikes the top of the LSC at increasingly oblique angles with successive reflections. This increases the chances of total internal reflection while reducing the distance light must travel in order to reach the solar cells. To assess the LSC performance parameters, the Monte Carlo method was employed.

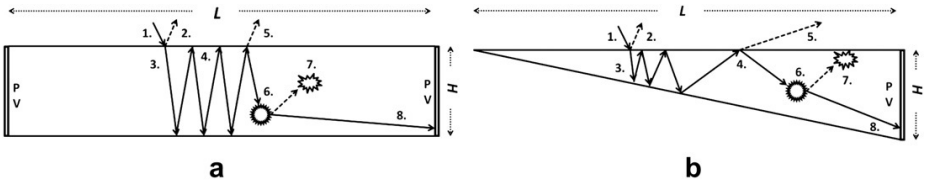

Figure 3.13: Typical events in (a) a planar and (b) a wedge-shaped LSC. The incident light (1) enters the top surface of the LSC where it is either reflected (2) or refracted in (3) light which enters the LSC may experience total internal reflection, (4) escape through the top surface, (5) be absorbed by the dye and re-emitted, (6) lost to the plastic matrix or dye, (7), or reach the PV cell (8). Reproduced from [12], Copyright (2013), with permission from Elsevier.

Overall, the planar LSC outperforms the wedge LSC in term of efficiently concentrating light when the sun is high in the sky, such as during early summer, with 3.5% for wedge LSC concentrator and 6.3% for the planar LSC However, when the sun

stays low in the sky, such as during early winter, the wedge LSC achieves a efficiency of 32.8% greater than that of the planar LSC at 7.6%.

Liu et al. [13] proposed a novel side-mounted concentrator solar module structure and design that could be more compact and thin, compared to current designs. The proposed design as shown in Figure 3.14 consists of a large flat panel of a certain thickness, which has two-dimensional micro-prism strips with a highly reflective coating at the bottom. One solar cell strip is attached to one of the two narrow ends of the concentrator. A method of ray-tracing simulation was used to investigate the efficiency of the designed concentrator. During the simulation, it is found that the density and shape parameters of the micro-prisms play a critical role for light-collecting efficiency. For this reason, optimization is necessary for improving efficiency. The optimization was carried out by changing some parameters such as the hemline and base-angle. Liu et al. proved that the proposed concentrator can provide perfect concentration efficiency with a Geometrical Concentration of greater than 2.7. Furthermore, the concentrator solar cell of this design is fully planar and easily expanded into a large cell mosaic-piling like panel. Most importantly, the design is very different from the traditional concentrator, where the concentrator panel is normally stacked over the solar cell. As a consequence, it is much easier to mechanically mount the solar cell chips to the concentrator with minimal alignment requirement.

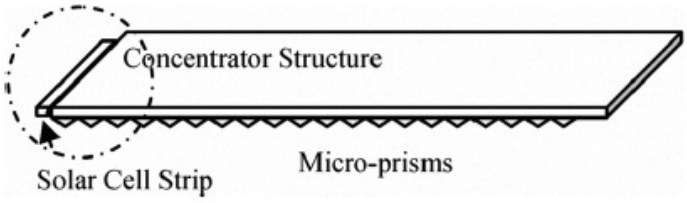

Figure 3.14: Schematic diagram of proposed concentrator with micro-prism structures [13]. Copyright ©2009, IEEE.

3.4 Summary

Based on the conducted survey in this chapter, the shape of the solar panel whether is internal or external has big effect on the solar panel performance. Some designs obtained a good improvement, but their cost and complexity increased as well. Arranging solar panels in arrays might maximize the output energy and minimize the cost. Many parameters should be taken into consideration. For instance, PV panel orientation, its tilt angle with the horizontal plane, and shadow effect. In the following chapters, the optimal design of solar farm which satisfies the above concerns will be proposed. This design will be done using multi-objective optimization techniques.

Chapter 4

Multi-objective Optimization

The chapter is organized as follows. After introducing some highlights about multi-objective optimization in Section 4.1. Section 4.2 illustrates the main concepts of multi-objective optimization. Section 4.3 introduces evolutionary multi-objective optimization (EMO) as a suitable method to solve MOPs. In addition, NSGA-II as well-known evolutionary MO approach used in this thesis, is explained in detail in Section 4.4.

4.1 Introduction

Multi-objective optimization has its roots in the nineteenth century as its first use in economics. Nowadays, multi-objective optimization is an important area especially in science and engineering. Most real-world search and optimization problems encountered in practice are multi-oobjective problems (MOPs). They normally have several (possibly conflicting) objectives that must be maximized/minimized at the same time. As the continuous increasing of the complexity of MOPs (e.g., number of objectives, dimension of the search space), many advanced multi-objective metaheuristics has been widely proposed to solve them.

4.2 Multi-objective Optimization Concepts

Multi-objective Optimization Problem (MOP) (also called multi-criteria optimization, multi-performance, or vector optimization problem) can be defined as the problem of finding: a vector of decision variables which satisfies constraints and optimizes a vector function whose elements represent the objective functions. These functions form a mathematical description of performance criteria which are usually in conflict with each other. Hence, the term "optimize" means finding such a solution

which would give the values of all the objective functions acceptable to the decision maker [33].

$$\text{MOP} = \begin{cases} min/max \;\; F(x) = (f_1(x), f_2(x), ..., f_n(x)) \\ s.c. \; x \in S \end{cases}$$

Where $n\,(n \geq 2)$ is the number of objectives, $x = (x_1, ..., x_k)$ is the vector representing the decision variables, and S represents the set of feasible solutions associated with equality and inequality constraints and explicit bounds. $(f_1(x), f_2(x), ..., f_n(x))$ is the vector of objectives to be optimized.

The optimal solution for MOPs is not a single solution as for mono-objective optimization problems, but a set of solutions defined as Pareto optimal solutions. A solution is Pareto optimal if it is not possible to improve a given objective without deteriorating at least another objective. Obtaining the Pareto optimal set and, consequently, the Pareto front is the main goal of the resolution of a multi-objective problem.

Assuming a minimization problem, an objective vector $u = (u_1, ..., u_n)$ is said dominated $v = (v_1, ..., v_n)$ (denoted by $u \prec v$) if and only if no component of v is smaller than the corresponding component of u and at least one component of u is strictly smaller, that is,

$\forall i \in \{1, ..., n\} : u_i \leq v_i \wedge \exists i \in \{1, ..., n\} : u_i < v_i$

4.3 Evolutionary Multi-objective Optimization (EMO)

Based on the principle of multiobjective optimization problems, evolutionary algorithms seem particularly suitable to solve these types of problems. Evolutionary

algorithms can deal simultaneously with a set of candidate solutions (the so-called population). As a result, it helps to find several members of the Pareto optimal set in a single run of the algorithm, instead of having to perform a series of separate runs as in the case of the traditional mathematical programming techniques. Besides, evolutionary algorithms are less susceptible to the shape or continuity of the Pareto front. For instance, they can easily deal with discontinuous or concave Pareto fronts, whereas these two issues are still a real concern for mathematical programming techniques.

4.4 Non-dominated sorting genetic algorithm (NSGA-II)

It is one of the popularly used EMO algorithms which attempt to find multiple Pareto-optimal solutions for a multi-objective optimization problem. It uses non-dominated sorting and a crowded-distance approach to find well spread solutions over the Pareto-optimal front[34]. Simplicity, effectiveness, modularity and low number of user-defined parameters, are the main factors determining the popularity of NSGA-II among other multi-objective optimization methods. The main components of NSGA-II are: elite-preserving operator (preserve and use previously found best solutions in subsequent generations), non-dominated sorting (the population order into a hierarchy of non-dominated Pareto fronts) and crowded tournament selection operator to preserve the diversity among non-dominated solutions in the higher stage of the run in order to obtain a good spread of solutions.

4.4.1 General Description of NSGA-II

The procedure of the NSGA-II is shown in Figure 4.1 and is as follows. First, a combined population $R_t = P_t \cup Q_t$ (of size $2N$) of the parent P_t and offsprings Q_t populations (each of size N) is formed. Then, the population R_t is sorted in nondominated fronts. Now, the solutions belonging to the best nondominated set, i.e. F_1 , are of best solutions in the combined population and must be emphasized more than any other solution. If the size of F_1 is smaller than N, all members of F_1 are inserted in the new population P_{t+1} . Then, the remaining population of P_{t+1} is chosen from subsequent nondominated fronts in order of their ranking. Thus, the solutions of F_2 are chosen next, followed by solutions from F_3 . However, as shown in Figure 4.1, not all the solutions from F_3 can be inserted in population P_{t+1} . Indeed, the number of empty slots of P_{t+1} is smaller than the number of solutions belonging to F_3 . In order to choose which ones will be selected, these solutions are sorted according to their crowding distance (in descending order) and, then, the number of best of them needed to fill the empty slots of P_{t+1} are inserted in this new population. The created population P_{t+1} is then used for selection, crossover, and mutation to create a new population Q_{t+1} , and so on for the next generations.

4.4.2 Detailed Description of NSGA-II

The main loop of NSGA-II procedure is shown in Algorithm 4.1. First, the parent population P_0 is initialized randomly based on the problem range and constraints. The population is sorted based on the non-domination. Each solution is assigned a fitness equal to its non-domination level (i.e. 1 is the best level). Then, the offspring population Q_0 is generated based on tournament selection, crossover, and mutation. Now, the current parent population is combined with the current offsprings and they

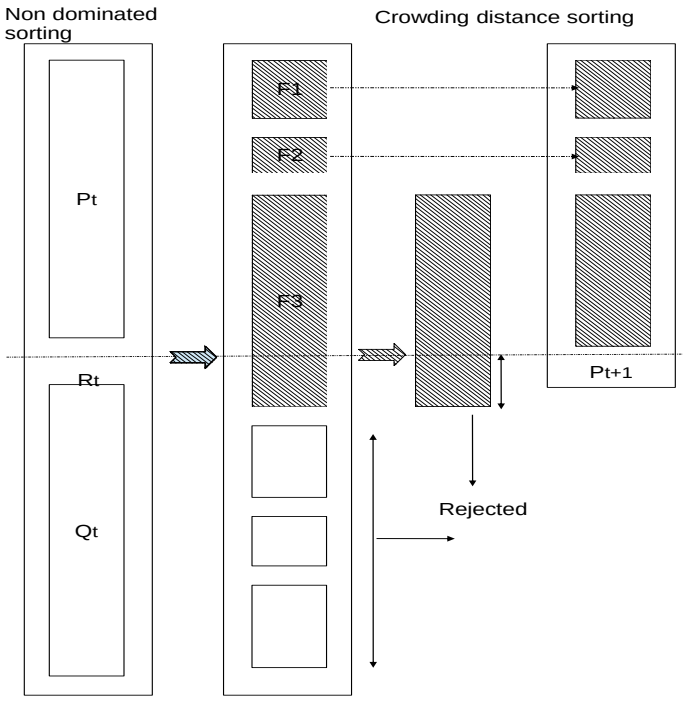

Figure 4.1: Illustration of the operation of NSGA-II.

are sorted again based on non-domination and only the best N individuals are selected. Non-dominated sorting is illustrated in Algorithm 4.2 as follow:

After the non-dominated sort is done, the crowding distance will be assigned. First, the distance for all the individuals is initialized to be zero. For each objective function, the population is sorted according to each objective function value in ascending order, and the boundary solutions are assigned an infinite distance value. All other intermediate solutions are assigned a distance value equal to the absolute normalized difference in the function values of two neighboring solutions. Finally, crowding-distance value is calculated as the sum of individual distance values corresponding to each objective. Figure 4.2, shows the crowding distance of the ith solution in its front (marked with solid circles). Also, Algorithm 4.3 outlines the crowding distance procedure as follow:

Algorithm 4.1 : NSGA-II Algorithm

Generate initial parent population P_0 (uniform random distribution)
for all individuals in the population **do**
  Evaluate objective values
  Evaluate constraints values
end for
Assign rank (level) based on Pareto dominance
Generate offspring population Q_0 based on
  Tournament selection
  Recombination and mutation
for $t = 1$ **to** number of generations **do**
  for all Parent and offspring population **do**
    $R_t = P_t \cup Q_t$ Combine parent and offspring population
    F = fast-non-dominated-sort(R_t) $F = (F_1, F_2, ..., F_i)$ all non-dominated fronts of R_t
    $i = 0$
    repeat
      crowding-distance-assignment(F_i)
      $R_{t+1} = P_{t+1} \cup F_i$ Include i_{th} non-dominated front in the parent pop
      i = i+1 Check the next front
    until $P_{t+1} + F_i \leq N$ until the parent population is filled
  end for
  sort(F_i, $\prec_n$) Sort in descending order using $\prec_n$
  Create next generation Q_{t+1} based on
    Tournament Selection
    Recombination and Mutation
end for

To choose the solutions to fill P_{t+1} of size N, the solutions sorted in descending order using crowded comparison operator $\prec_n$ based on non-domination rank p_{rank}, and crowding distance $F_i(d_j)$. And, the comparison is carried out as below:

$$\boxed{\text{p} \prec_n q \text{ if } (p_{rank} < q_{rank}) \text{ or } ((p_{rank} = q_{rank}) \text{ and } (F_i(d_p) > F_i(d_q)))}$$

Finally, the new population P_{t+1} of size N used to create next generation Q_{t+1} based on selection, crossover, and Mutation.

Constraints are handling based on the dominance relationship taking into consideration constraint values besides objective values. A constraint-domination $\prec_c$ is

Algorithm 4.2 : non-dominated sorting

```
for each individual p in main population P do
    S_p = φ                    Contains all the individuals that is being dominated by p
    n_p = 0                    Number of individuals that dominate p
end for
for each individual q in P do
    if p ≺ q then
        S_p = S_p ∪ {q}                Add q to the set of solutions dominated by p
    else if q ≺ p then
        n_p = n_p + 1                  Increment the domination counter of p
    end if
    if n_p = 0 then
        p_rank = 1                     p belongs to the first front
        F_1 = F_1 ∪ {p}
    end if
    i = 1                          Initialize the front counter
    while F_i ≠ φ do
        Q = φ                          Used to store the members of the next front
        for each p ∈ F_i do
            for each q ∈ S_p do
                n_q = n_q − 1
                if n_q = 0 then
                    q_rank = i + 1             q belongs to the next front
                    Q = Q ∪ {q}
                end if
            end for
        end for
        i = i + 1
    end while
    F_i = Q
end for
```

defined as $\vec{x}_1$ constraint-dominates $\vec{x}_2$, i.e., $\vec{x}_1 \prec_c \vec{x}_2$ iff any of the following conditions is true:

- $\vec{x}_1$ is feasible and $\vec{x}_2$ is not.
- $\vec{x}_1$ and $\vec{x}_2$ are infeasible and $\vec{x}_1$ dominates $\vec{x}_2$ in constraint function space.
- $\vec{x}_1$ and $\vec{x}_2$ are feasible and $\vec{x}_1$ dominates $\vec{x}_2$ in objective function space.

Algorithm 4.3 : Crowding distance mechanism

Require: F Non-dominated set
$N_s = |F|$ Number of solutions in the non-dominated set
M = Number of objective
$F(i).dist = 0 \quad \forall \quad i = 1, 2, ...\mathrm{N}_s$ Initialize distance
for $m = 1$ **to** M **do**
$F = sort(F, m)$ Sort based on objective value
$F(1).dist = F(N_s).dist = \infty$ Assign infinity to the corner points
for $i = 2$ **to** $(N_s - 1)$ **do**
$F(i).dist = F(i).dist + (F(i+1, m) - F(i-1, m))/(f_m^{max} - f_m^{min})$ Calculate $F(i).dist$ based on neighboring points
end for
end for
Higher dist ⇒ Higher rank

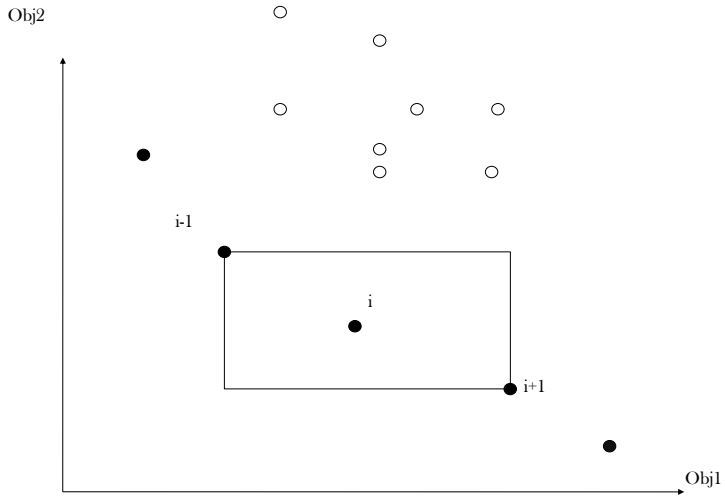

Figure 4.2: Crowding-distance calculation. Points marked in filled circles are solutions of the same non-dominated front.

4.5 Summary

This chapter introduced the fundamental concepts of multi-objective optimization. NSGA-II provided in detail as one of the most efficient evolutionary algorithms to solve muti-objective optimization problems. In the next chapter, NSGA-II will

be employed to solve a real-world problem with two objectives, namely, maximum incident energy and minimum of the deployment cost.

Chapter 5

Photovoltaic in Farming

The main focus of the thesis is presented in this chapter. First, some approaches for enhancing the received energy of PV system are reviewed in Section 5.1. The first approach is the estimation of optimum tilt angle experimentally or using mathematical models. The second approach is using PV with Sun tracking system. Section 5.2 reviews some related works in the first part. Then, the proposed farm design is described formally in the second part.

5.1 Introduction

Solar panels are arranged in arrays to maximize the output energy. These arrays need to be spaced out to reduce the shading effect as the Sun moves and the array orientations change, so more land area is needed. They also require more complex mechanisms to keep the array surface at the required tilt angle. Depending on the application, PV arrays need to be mounted at a fixed inclination or tracking the Sun in its daily orbit across the sky. In this section, a few studies about fixed and Sun tracking PV systems are provided.

5.1.1 Estimation of optimum tilt angle

The tilt angle plays very important role on the solar energy received by the system. For instance, a system mounted at horizontal position does not receive the same amount of energy as a system at vertical position does. On other words, the tilt optimal angle is commonly considered as the one that affects the solar energy collected annually [35].

Asowata et al. [36] conducted a study to optimize the available output power from a PV panel for a specific point of latitude in South Africa. Mathematical models and simulation packages in combination with experimental data were used to

determine the optimum tilt and orientation angles. Determining the optimum tilt angle involves placing the PV panel at an orientation angle of 0^0 and changing the angle of tilt to 16^0, 26^0, and 36^0, respectively. These angles are derived from the Heywood and Chinnery Equations of latitude for calculating tilt angles of PV panels in South Africa. According to their results, the authors indicated that tilt angles between 26^0 and 36^0 provided optimum photovoltaic output power for winter months in South Africa.

Kaldellis and Zafirakis [37] investigated the optimum tilt angle for PV panels operating in Athens, central Greece during the summer period. To achieve that, two PV arrays arranged into two pairs, six panels each. The twelve panels of the installation are connected in six parallel strings of two. The orientation of these PV panels is fixed with the azimuth angle set equal to zero. The PV configuration used for the experimental measurements is installed at the geographical coordination of 37^0 $58^{'}$ N and 23^0 $40^{'}$ during the hot period of the year (from mid-May to mid-September). Measurements took for different angle of the variable angle PV pair (0^0, 15^0, 30^0, 45^0, 60^0, and 75^0), while the fixed angle PV pair kept at 15^0. According to the obtained results, the angle of $15^0(\pm 2.5^0)$ was as optimum for almost the entire summer period. The comparison of the daily performance between the fixed and the variable PV panels tilt angles was through estimation of the relative capacity factor "CF_{PV}" deviation. According to the obtained results, performance deviation was depended on the selected tilt angle and the period of examination, with the greatest deviation (i.e. 27.3%) between the fixed and the variable tilt angle PV pairs.

Mraoui et. al [38] examined the effect of tilt angle on the received and produced energy for Algiers and Ghardaa. They employed FORTRAN programing language with some mathematical Equations to calculate the solar energy received and produced by the PV panel per unit area based on the tilt angle. First, the program reads

radiometric data for the chosen city for each hour of the year varying from 1 to 8670. Then, the position of the sun in the sky is calculated using the geographical position of the site. For a selected tilt angle, the incidence angle of the sun vector on the inclined solar collector is calculated. The results showed that the angle maximizing the received monthly average minimum energy is close to $latitude + 23^0$ in Algiers and close to $latitude + 10^0$ in Ghardaa. Overall, choosing tilt angle equal to $Latitude + 23^0$ allows increasing the average minimum energy by up to 12%.

Chandrakar and Tiwari [39] presented a simple mathematical procedure based on the monthly horizontal radiation to estimate the tilt angle at Chhattisgarh in India. They found that the optimum tilt angle for the winter months is 37^0 and for the summer months is 12^0. Overall, the yearly average tilt panel is 23.5^0 which close to the latitude of Chhattisgarh site (24.5^0).

5.1.2 PV with Sun tracking system

The incident radiation on a stationary PV panel is changing due to the continuous change in the relative position of the Sun and the Earth. Also, reaching a maximum amount energy happens when the direction of the solar radiation is perpendicular to the PV panel surface. In this context, for maximum efficiency of a PV panel, it is necessary to have it equipped with a sun tracking system. Trackers need not point directly at the Sun to be effective. If the aim is off by 10^0, the output is still 98.5% of that of the full-tracking maximum. In the cloudiest and haziest locations, the gain in annual output from trackers can be in the low 20% range. In a generally good area, annual gains between 30% and 40% are typical. The gain in any given day may vary from almost zero to nearly 100% [40].

Many solar tracking systems have been proposed to facilitate the above tasks over the past few years. These systems can be classified into several types according

to several criteria. A first classification can be based on the number of rotation axes (single-axis, and dual-axis). Another classification depends on the orientation type (e.g. NS, EW,... etc.). Finally, depending on the tracker activity type, a solar tracker can be active or passive [41]. In this section, some of these tracking systems are reviewed.

Khalifa and Al-Mutawalli [14] conducted an experimental study to investigate the effect of using a two-axis sun tracking system on the thermal performance of compound parabolic concentrators (CPC). The tracking system was designed to track the Sun position every three to four minutes in the horizontal plane and every four to five minutes in the vertical plane. As shown in Figure 5.1, the tracking system comprises of two identical sub-systems, one for each axis, with each sub-system consisting of two adjacent photo-transistors separated by a partition of a certain height. A difference amplifier activates the DC motor through a driving circuit which used to drive the collector around the desired axis until the voltage between two photo-transistors is zero. This indicates that the Sun's rays becomes normal to the collector surface. It was shown that the tracking system had a power consumption of just 0.5 Wh and yielded an improvement of around 75% in the collected solar energy, compared to a fixed collector of equivalent dimensions.

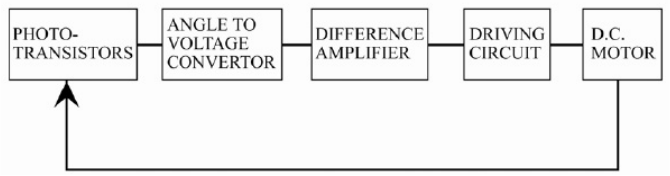

Figure 5.1: Block digram of the sun tracking system. Reproduced from [14], Copyright (1998), with permission from Elsevier.

Chicco et al. [42] estimated the production of three Sun tracking plants located in different sites, compared with the production of fixed PV modules. The first site consists of 15 individual systems, each of which with one coordinate-controlled

tracking were compared with a 0^0 azimuth and 36^0 elevation angles as fixed cases. The second site consists of 90 individual systems, each of which with separate coordinate-controlled tracking were compared with a 0^0 azimuth and 30^0 elevation angles as stationary cases. For the last site, the position of the Sun-tracking system is updated every 15 minutes; whereas, the fixed system maintained at a tilt angle of 30^0 with 35^0 elevation angle. The results showed that the average improvement of using the Sun-tracking system are 32.9% and 35.1% for the simulated values and 37.7% and 30.4% for the actual data for the first and second sites, respectively. For the third site, the Sun-tracking system yields an annual improvement of 31.5% for the Sun-tracking system.

Karimov et al. [15] designed a PV tracking system with four rotating modules which is hold by a pyramidal stand. The upper edge of the pyramidal stand is a rotor with fixed length, and other two edges are variable in length in order to fix the inclination angle of modules at 23^0, 34^0 and 45^0. The solar modules were divided into two pairs and the angle between the modules of a pair was 170^0 (Figure 5.2). Karimov et al. showed that the output voltages in the morning and in the evening are not different for the tracking modules; whereas the output voltages at noon are larger than the voltages at any other time for the fixed modules. Furthermore, the tracking modules produced 30% more energy compared with the fixed modules

Aliman et al. [43] developed a new structure of sun tracking to gain high concentration solar energy. The tracking system consists of mirrors which are arranged in rows and columns. A master mirror surrounded by slave mirrors which reflect sun rays into the same fixed target of the master. Then, the master mirror reflects sun beams to a stationary target, and it acts as a reference for all the slave mirror images. Sun tracking has two tracking axis that are perpendicular to each other. First rotational axis is pointing toward the target. The other axis, elevation axis is attached

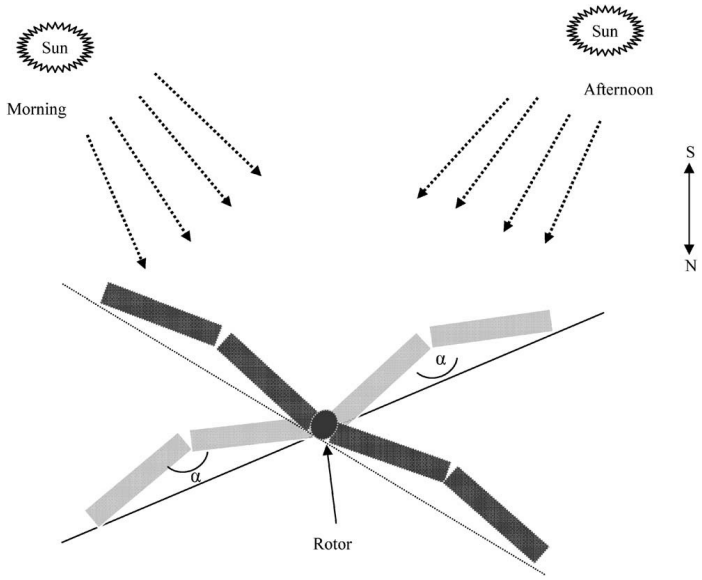

Figure 5.2: Positions of PV solar tracking system modules in morning and afternoon hours. Reproduced from [15], Copyright (2005), with permission from Elsevier.

parallel to the reflector. The proposed tracking system proved experimentally to be promising and it was less complicated and low cost compared to the conventional two-stage solar reflector system.

Abu-Khader et. al. [44] investigated the operation and the effects of using multi-axis (NS, EW, vertical) sun tracking systems Electrical generation of a flat photovoltaic system (FPVS) at various modes in Jordan. The results showed that a high power was almost always observed at NS tracking. Also, the use of multi-axis sun tracking systems enhances the total power output by 30% to 45% compared to fixed solar systems.

5.2 Optimal PV Farm Design

Even though the most common and widespread PV panels are flat, the power that they produce varies over the course of the day as the Sun position changes. For this reason, the panels are mounted on tracking systems to keep track of the Sun,

which add complexity and expense.

In [45], Faiman curved flat solar panels by bending them into parabolic dishes in order to maximize the efficiency of the solar panels and minimize the economic and environmental cost of producing solar power, one of the crucial barriers to the field's development.

In the current work, we used Faiman's idea for curving the flat solar panels into parabolic trough panels. We have utilized multi-objective optimization algorithm to design an optimal solar field with parabolic trough collectors.

5.2.1 Related Work

Maximum energy output of a field of collectors may be one of the objectives of a solar plant design. Other objectives may be minimum plant cost or minimum produced energy cost. The design of a field of collectors is therefore a multi-objective optimization problem. Most recent optimization works applied to design solar farm systems are presented in this section.

Appelbaum and Weinstock [18] formulated a solar collector field design as an optimization problem. They applied constraints optimization techniques to obtain optimal design parameters of the solar field (optimal number of rows, distance between collector rows, collector height and collector inclination angle) that produce maximum annual energy, minimum field area (length and width), and maximum energy per unit collector area from a given field. The authors employed the Sequential Quadratic Programming for optimization. As a result of their experiment, it is possible to obtain a yearly energy increase of about 20% and a decrease of about 15% in the field area (depending on the row distance).

The work in [46] is a similar to [18]; however, Bourennani et al. [46] utilized Differential Evolution (DE) and simulation-based optimization methods to compare

the maximum annual incident energy captured by the solar collectors. DE is an effective evolutionary algorithm that appears to be robust in solving many engineering problems. In [46], four variables are to be addressed for optimal design: the distance between the solar panels, the inclination of the PV panels, the height of a PV panel, and the number of rows (a discrete variable). To validate the results, they compared the DE results to a simulation-based optimization approach. According to the findings of Bourennani et al., DE algorithm offered a better performance than the simulation approach for solving this mixed-type variable problem with constraints.

In the early work [47], Vaile and Summerer proposed a multi-objective optimization of a combination of ground solar power plants with space-based solar plant in order to gratify the electricity demands of Europe. The optimization is performed with a multi-agent-based optimizer called EPIC [48] to minimize the cost of the overall system and to maximize the provision-reliability of electric power for an entire day. Orbital parameters, architecture of the spacecraft, size of the terrestrial plant, and size of the terrestrial storage system are optimized for minimizing cost per kW.

Khalkhali et al. [49] used multi-objective genetic algorithms (GAs) for optimization of a solar system using modified NSGA-II algorithms. The two conflicting objectives to be optimized simultaneously are maximizing net energy stored and minimizing time of Phase Charge Material (PCM). The decision variables consisted in inner diameter of pipes, area of collectors, water mass flow rate, tilt of collector and the mass of PCM. Deb et al. [50] solved a four-objective optimization model of a solar thermal power plan system. Profits, total investment costs, internal rate of return and global emissions were the four objective functions. Firstly, they found a set of trade-off solutions over the entire Pareto-optimal front using a clustered NSGA-II algorithm. After that, a reference point based a multiple criterion decision making (MCDM) approach with the clustered NSGA-II used to focus on preferred on some

parts of the Pareto-optimal front, rather than attempting to find points on the entire front. Deb et al. showed that a multi-objective optimization procedure and decision making can be used together to consider trade-off solutions and eventually lead to a single preferred solution.

Kornelakis [51] developed a multi-objective technique based on Particle Swarm Optimization (PSO) algorithm to achieve the optimal design of photovoltaic grid-connected systems (PVGCSs). His goal was to maximize the PVGCS total net profit and the PVGCS total environmental benefit. The optimization's decision variables are the number of the PV modules, PV's tilt angle, placement of the PV within the available installation area and the optimal distribution of PV among the DC/AC converters. Myers et al. [52] combined a generic algorithm method and a code in order to obtain optimal 3D-PV shapes. Nasiraghdam and Jadid [53] presented a novel multi-objective artificial bee colony algorithm to solve the distribution system reconfiguration and hybrid (photovoltaic/wind turbine/fuel cell) energy system optimal sizing. The objectives to be optimized include power loss, the total cost and total, emission minimization, and the voltage stability index (VSI) maximization. In their algorithm, Nasiraghdam and Jadid used crowding distance operator to preserve the diversity in the archive of Pareto solutions. Compared with NSGA-II and MOPSO methods the obtained solutions from the proposed algorithm have a good quality and a better diversity of the Pareto front. Suchitra et al. [54] developed a hybrid system consists of Photovoltaic panels, a diesel generator and batteries. They used multi-objective optimization (NSGA-II) to minimize total net present cost and pollutant emissions. Four variables to be optimized were type of PV panels, number of PV modules in parallel constituting the panel, type of battery and the number of batteries in parallel constituting the battery pack.

Ibrahim et al. [19] used and compared two multi-objective evolutionary algo-

rithms (MOEAs) called Non-dominated Sorting Genetic Algorithm-II (NSGI-II) and Generalized Differential Evolution Generation 3 (GDE3) to design an optimal PV farm in Toronto. The objectives were maximizing the total incident solar energy and minimizing the cost of PV panel deployment in a specific field. Six decision variables to be optimized were the number of collector rows, distance between collector rows, dimension of collectors, collectors inclination angle, and collectors azimuth angle.

Rao et al. [21] presented the optimal design of stationary multirow compound parabolic concentrator (CPC) solar collectors with considering the shading effect. They used a modified game theory (MGT) methodology for the solution of the three objective constrained optimization problems. These objectives were maximization of the annual average incident solar energy, maximization of the lowest month incident solar energy, and minimization of the cost. besides, eight decision variables included distance between two neighboring rows, dimension of collectors, collectors inclination angle, receiver length, half of the acceptance angle, truncation ratio, number of rows, and number of CPC in each row. Compared with the optimum flat plate solar collectors, the CPC solar collector could reduce the value of cost per unit energy ratio. The cost per unit energy reduced as much as 41% depending on different land prices if the total energy output can be sacrificed by about 20% compared to the flat plate solar collector system.

The work in this thesis is inspired from the work in [19]. The main distinct difference is that Ibrahim et al. [19] have used flat solar panels in their farm design; whereas, we have used parabolic trough panels. In addition, we added another decision variable to the optimization problem which is the rim angles of the collectors. NSGA-II, well known multi-objective evolutionary algorithm, is used to find a spectrum of trade-off feasible solutions. Six decision variables are to be found for an optimal design: the number of collector rows (a discrete variable), the center to

center distance among rows (pitch), the rim angle of the collectors, the inclination of the PV panels, the height of a PV panel, and collector's clearance above ground.

5.2.2 The Proposed Model

The optimal design of a solar field may be formulated mathematically as a multi-objective optimization problem. The objective is maximizing the absorbed solar energy with minimum cost. Solar field as shown in Figure 5.3 is considered for this thesis. The field consists of parallel rows of collectors which are facing roughly the south and inclined at an angle β. Each row has equal number of identical collectors connected in series. The aperture area of each row is assumed to be having length L and height H; the center-to-center distance between rows is p (pitch). The length of the collectors L is equal to the length of the field, and the width is W. There should be a minimum clearance of E above the ground to minimize the collectors of dust, debris, or snow.

5.2.2.1 Mathematical Modeling of the Solar Field

The height of the collectors above the ground should be limited for maintenance purpose. Furthermore, the height H of the collectors themselves is limited by the manufacturer [18], [55]. Also, the center-to-center distance among rows P is limited to allow easy access among PV panels [16]. Thus,

$$H^{'} + E \leq A_{max} \tag{5.1}$$

$$H \leq H_{max} \tag{5.2}$$

Where $H^{'} = H \times \sin\beta$,

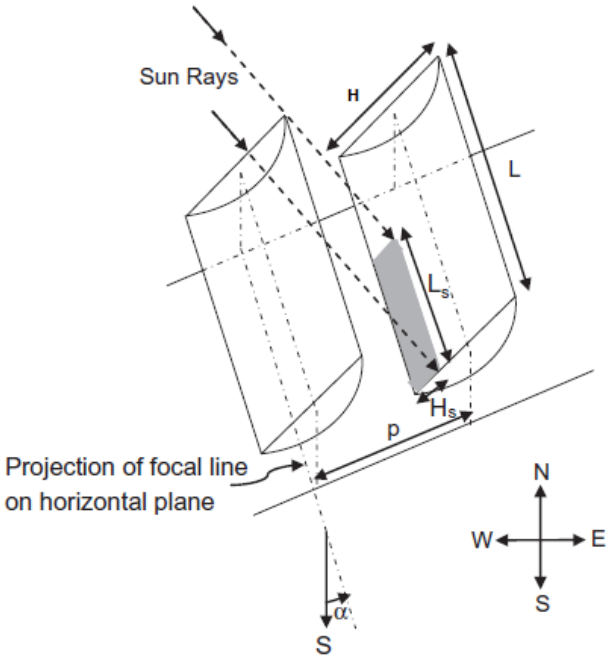

Figure 5.3: Collectors arrangement in a stationary solar field. Reproduced from [16], Copyright (2005), with permission from Elesvier.

A_{max} is the maximum collector height above ground.

β as shown in Figure 5.4 is the collector inclination angle.

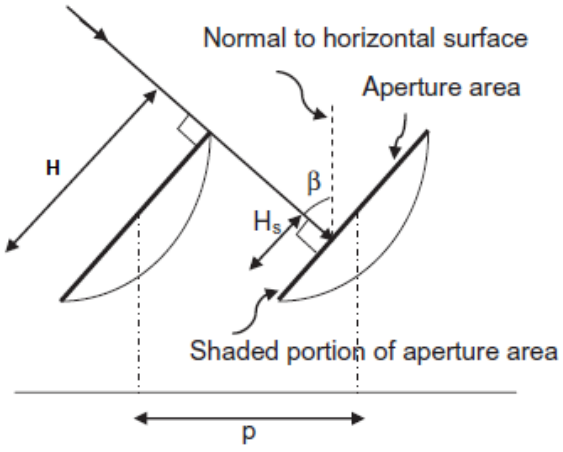

Figure 5.4: Collector inclination angle (β). Reproduced from [16], Copyright (2005), with permission from Elesvier.

γ is the surface azimuth angle which depends on solar azimuth angle (γ_s) and

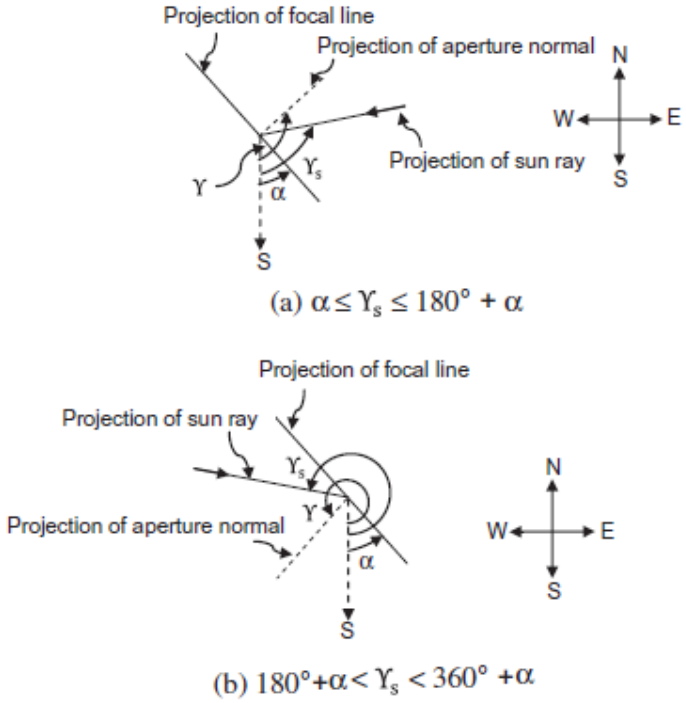

Figure 5.5: Plan view of the collector shows surface azimuth angle γ and solar azimuth angle γ_s. Reproduced from [16], Copyright (2005), with permission from Elesvier.

field orientation angle (α).

In order to find its expression, Figure 5.5 shows plan view of ray geometry at the collector row. From the geometry shown in Figure 5.5, the following expression of γ is derived [16].

$$\gamma = \begin{cases} 90^0 + \alpha & \text{if } \alpha \leq \gamma_s \leq 180^0 + \alpha \\ 270 + \alpha & \text{if } 180^0 + \alpha < \gamma_s < 360^0 + \alpha \end{cases} \tag{5.3}$$

Because the N−S orientation leads to the highest energy availability and the lowest cost of electricity [56] [16], in this case $\alpha = 0$ (field orientation angle). Then, the bounds of γ_s which illustrated in Figure 5.5 and the value of γ in Equation 5.3 will change as follows:

$$\gamma = \begin{cases} 90^0 & \text{if } 0^0 \leq \gamma_s \leq 180^0 \\ 270 & \text{if } 180^0 < \gamma_s < 360^0 \end{cases} \tag{5.4}$$

The expression of solar azimuth angle (γ_s) is given by [16]:

$$\gamma_s = \begin{cases} -\cos^{-1}\left[\frac{\cos\theta_z \sin\phi - \sin\delta}{\sin\theta_z \cos\phi}\right] & \text{if } -180^0 \leq \omega \leq 0^0 \\ \cos^{-1}\left[\frac{\cos\theta_z \sin\phi - \sin\delta}{\sin\theta_z \cos\phi}\right] & \text{if } 0^0 \leq \omega \leq 180^0 \end{cases} \tag{5.5}$$

Where

$$\theta_z = cos^{-1}(cos(\phi)cos(\delta)cos(\omega) + sin(\phi)sin(\delta)) \tag{5.6}$$

$$\delta = 23.45 \sin(360(\frac{284+n}{365})) \tag{5.7}$$

$$n = \text{day of the year}$$

$$\omega = (Solartime - 12) \times 15 \, [17] \tag{5.8}$$

Height of the shadow cast by one row on the other at any time can be written down as

$$H_s = \left[H - (P\cos\beta)\right]^+ \tag{5.9}$$

And, the length of the shadow cast by one row on the other is as follows:

$$L_s = \left[L - \left|P\tan(\gamma - \gamma_s)\right|\right]^+ \tag{5.10}$$

Then, area A_s of shadow with height H_s and length L_s is written as:

$$A_s = \begin{cases} H_s L_s & \text{if } \theta_z \leq 90^0 \\ 0 & \text{otherwise} \end{cases} \tag{5.11}$$

The relative shaded area a_s as indicated in Figure 5.3 is given by [16]:

$$a_s = \begin{cases} h_s l_s & \text{if } \theta_z \leq 90^0 \\ 0 & \text{otherwise} \end{cases} \tag{5.12}$$

where,

$$l_s = L_s/L = \left[1 - \left|\frac{P/H}{L/H}\tan(\gamma - \gamma_s)\right|\right]^+ \tag{5.13}$$

and

$$h_s = H_s/H = \left[1 - (\frac{P}{H}\cos\beta)\right]^+ \tag{5.14}$$

$0 \leq h_s \leq 1$, and $0 \leq l_s \leq 1$.

Concept of shading is relevant only when sun is present in the sky when $\theta_z \leq 90^0$. For non-sunshine hours, shaded areas are considered to be zero.

The incidence angle θ is the angle between a normal to the collector face and the incoming solar beam given by [56]

$$\cos\theta = \cos\delta\left[\sin^2\omega + (\cos\phi\cos\omega - \tan\delta\sin\phi)^2\right]^{\frac{1}{2}} \tag{5.15}$$

The yearly amount of energy E_{inc} incident on unit aperture area of trough over a period of time, without considering shading (first row) can be written as [16]:

$$E_{inc} = \sum_{n=1}^{365}\sum_{T_R}^{T_S}\left[(I_{bn})\cos\theta \times \Delta T\right] \tag{5.16}$$

The yearly amount of energy E_{avl} incident on unit aperture area of trough over a period of time, with considering shading ((K-1) row(s)) can be calculated as [16]:

$$E_{avl} = \sum_{n=1}^{365} \sum_{T_R}^{T_S} \left[(1 - a_s)(I_{bn}) \cos\theta \times \Delta T \right], \tag{5.17}$$

where ΔT is the summation time interval from sun rise T_R to sunset T_S on the collector for the beam irradiance. The outer summation represents one year term from January 1^{st} (n = 1) to December 31^{st} (i.e., n = 365).

5.2.2.2 Description of The Problem

Our multi-objective optimization PV parabolic trough design is six dimension (6D) problem with mixed-type integer and real variables. Thees variables have different ranges of values which make the problem more complex. The two objective functions are multimodel because they include trigonometric functions which are harder to solve. The Pareto front geometry as shown in Figure 6.1j is linear and curved convexity at the extreme. Also, the problem has two inequality constraints, and one complex equality constraint.

5.2.2.3 Objective, Variables, and Constraints

Our optimization problem to be solved consists of two objectives, six variables, two inequality constraints, and one equality constraint as described in Equations 5.1 to 5.22. The two objectives to be optimized as shown in Equations 5.18 and 5.19, respectively, are maximization of incident energy and minimization of the installation and material cost. The design variables are: the number of collector rows (K), the center-to-center distance between collectors (P), dimension of collectors, collectors inclination angle (β), surface azimuth angle (γ), and the rim angle of the collectors

(ψ). The variable domains are described below in Equations 5.23 to 5.28.

$$max\ Q = S \times L \times [E_{inc} + (K-1)(E_{avl})] \tag{5.18}$$

$$min\ C = S \times L \times K \times P_r \tag{5.19}$$

$$s.t.\ K \times H \times \cos\beta + (K-1) \times (P-H) \leq W \tag{5.20}$$

where S is the length of the parabola that is the cross-section of the trough, as described in Section 2.1.

$$H^{'} + E \leq A_{max} \tag{5.21}$$

$$H = f\left(-\frac{4}{\tan(\psi)} + \sqrt{\frac{16}{\tan^2(\psi)} + 16}\right) \tag{5.22}$$

Variable bounds:

$$2 \leq K \leq 10 \tag{5.23}$$

$$0.2 \leq H \leq 2 \tag{5.24}$$

$$0^0 \leq \beta \leq 90^0 \tag{5.25}$$

$$20^0 \leq \psi \leq 150^0 \tag{5.26}$$

$$1 \leq P \leq 4.5 \tag{5.27}$$

$$0.5 \leq E \leq 2 \tag{5.28}$$

Where

K $\in \mathbb{Z}^+$

H, β, P, E, $\psi \in \mathbb{R}$

5.2.2.4 Database

The location selected for all the experiments is Toronto, Ontario, Canada (Latitude 43.45^0 / Longitude -79.25^0). In Appendix A, Table A.1 shows 30 years of monthly averaged hourly direct normal beam irradiance in kWh/m^2 [57].

5.2.2.5 PV Panels

There are numerous types of PV panels in the market. PV panels are priced based on their electrical characteristics (Rated power, Voltage, Current, Module efficiency, Short-circuit current, Open-circuit voltage, Maximum series fuse rating, Maximum system voltage) and mechanical characteristics (Dimensions, Weight, Frame, number of Solar Cells). For our experiment, we have assumed that solar panel priced at \$372.70/m^2 for flat and parabolic farm designs.

Chapter 6

Results and Discussion

This chapter shows the obtained results of the optimal design of flat and parabolic trough solar collector systems. A comparison between the performance of both designs is discussed in detail.

Due to stochastic nature of MOEAs, NSGA-II is run 50 times each independently for both parabolic and flat designs. The stopping criteria for both algorithms is calling 5×10^4 function evaluations. The best solutions for both designs were compared properly. Also, parameter settings of NSGA-II are presented in Table 6.1.

Table 6.1: NSGA-II parameters' settings.

Population size	100
Initial population	Uniform Random
Maximum Function Evaluation	5×10^4
Mutation probability	1/6
Crossover probability	0.9
Mutation distribution Index	20
Crossover distribution Index	20
Runs	50

First, we developed our NSGA-II algorithm using MATLAB and it run on Intel(R) Core(TM) i5, CPU@2.40GHz. The optimum design of flat plate solar collector system implemented based on [18] and [19] studies. Tables 6.2 and 6.3 show the best obtained set of 100 non-dominated solutions (i.e., Pareto-front solutions) after 50,000 function evaluations using NSGA-II for flat and parabolic designs, respectively. Besides, Figures 6.1 and 6.2 show the Pareto-front set of non-dominated solution set for parabolic and flat plate with respect to number of collector rows.

Based on the given objectives and constraints of both designs, the execution time of the parabolic design was almost 60% higher than the execution time of the flat design. This happened because we modified the two objectives in the case of the parabolic design. We added a new parameter, S, which is the length of the cross-section of the trough to calculate the surface area of the parabolic collector. This modification made the problem more complex with adding new trigonometric functions (log and square root) which are harder to calculate.

To give more time for the designed model to find the solution, we have run the optimizer for $50,000 \times 1.6$ function evaluations for both models. As a result, no more improvement happened (just very small fractions increased).

Table 6.2: The Pareto-front set of non-dominated solution set found by NSGA-II for flat design.

K	H(m)	$\beta(^0)$	D(m)	$\gamma(^0)$	E(m)	Q(MWh)	Cost($)
2	0.20	27.53	2.50	-4.00	0.70	4.19	1118.10
2	0.20	27.53	2.50	-4.00	0.52	4.19	1118.10
2	0.64	23.78	2.50	-4.00	0.70	13.35	3572.82
2	2.00	26.06	2.50	-15.86	0.54	41.61	11193.82
2	0.78	23.74	2.38	-8.60	0.67	16.69	4480.21
2	1.92	26.06	2.31	-15.15	0.55	43.96	11841.15
2	2.00	26.06	2.31	-15.15	0.55	45.80	12342.79
2	0.20	25.76	2.50	-4.34	0.59	4.64	1240.40
2	1.72	25.29	2.09	-14.89	0.59	40.43	10893.28
2	0.73	23.72	2.29	-5.19	0.66	18.47	4954.52
2	1.24	27.72	2.42	-14.07	0.50	31.98	8593.89
3	0.60	27.53	1.84	-3.97	0.51	15.88	4251.74
3	1.49	22.50	2.09	-5.10	0.64	39.33	10602.69
3	0.85	28.08	2.14	-13.87	0.62	23.00	6171.88
3	1.92	27.78	2.05	-14.05	0.56	52.27	14131.08
3	0.20	27.39	2.50	-4.00	0.56	5.54	1478.39
3	0.49	28.19	2.14	-3.54	0.50	13.66	3659.05
3	0.45	31.93	2.16	-39.33	0.50	12.16	3377.43
3	1.83	24.00	2.31	-5.19	0.66	51.16	13795.49
3	0.97	27.53	1.84	-3.97	0.51	27.45	7370.20
3	0.27	27.53	2.50	0.05	0.50	7.63	2062.71
3	0.37	27.80	2.46	-10.25	0.52	10.70	2874.77
3	1.68	32.53	2.46	-5.20	0.53	48.50	13145.11
3	1.11	30.30	2.11	-13.97	0.60	33.08	8911.63
3	1.78	23.00	2.44	-5.20	0.58	54.13	14595.78
3	1.93	23.00	2.44	-5.71	0.54	58.69	15832.19
3	1.66	22.48	2.18	-5.10	0.64	50.50	13626.69
3	1.92	27.04	1.09	-5.42	0.54	59.70	16324.09
3	0.80	23.93	1.86	-5.21	0.65	25.42	6831.20
3	0.23	11.46	2.32	-4.00	0.51	7.32	2016.52
3	1.51	22.48	2.15	-7.70	0.64	48.87	13200.97
3	1.89	23.15	2.29	-5.20	0.56	61.88	16708.56
3	1.89	22.67	2.50	-5.20	0.63	64.07	17293.93
3	1.91	22.46	1.85	-5.20	0.56	64.84	17554.13
3	1.93	23.07	2.16	-15.86	0.50	65.75	17777.31
3	2.00	26.70	1.76	-5.92	0.63	68.64	18619.35
3	1.89	27.40	2.50	-5.20	0.58	67.18	18139.67
3	1.61	27.40	2.50	-5.20	0.64	57.47	15492.03
4	1.17	24.75	1.15	-8.69	0.65	42.59	11542.62
4	2.00	27.40	1.70	-5.20	0.50	73.61	20010.49
4	1.47	28.56	2.09	-3.83	0.50	54.58	14724.60
4	1.43	28.49	2.09	-3.83	0.57	53.11	14322.95
4	1.90	21.89	1.42	-7.54	0.54	70.08	19077.08

4	1.23	31.55	1.66	-6.72	0.60	46.73	12684.00
4	1.89	21.61	1.58	-5.78	0.50	71.84	19495.05
4	0.75	24.38	1.72	-8.69	0.65	28.85	7761.82
4	1.17	24.81	1.15	-8.69	0.68	45.49	12331.87
4	0.98	27.40	1.70	-5.20	0.50	39.04	10516.72
4	1.94	24.01	0.94	-9.52	0.73	76.25	21082.74
4	0.75	19.89	0.94	-5.06	0.87	29.90	8101.06
4	1.17	30.09	2.50	-13.92	0.55	47.78	12870.56
4	2.00	24.01	0.94	-6.80	0.63	81.01	22231.24
4	1.97	22.27	1.33	-7.54	0.61	80.40	21929.23
4	1.34	28.60	2.24	-6.72	0.59	55.93	15089.51
4	0.82	25.91	1.01	-5.21	0.54	34.11	9219.88
4	1.91	27.80	1.33	-7.54	0.58	79.00	21618.20
4	2.00	22.85	1.09	-16.96	0.54	83.16	22795.50
4	1.97	22.34	1.42	-7.54	0.61	82.61	22511.04
4	2.00	24.01	0.94	-6.80	0.63	85.52	23482.24
4	1.75	23.40	1.07	-8.03	0.58	75.59	20660.82
4	1.83	23.40	1.07	-14.08	0.58	78.91	21582.07
4	1.93	20.48	1.14	-10.27	0.53	84.66	23252.63
4	2.00	24.18	0.80	-6.80	0.69	89.38	24641.16
4	1.90	20.48	1.14	-5.60	0.56	87.09	23779.87
5	0.66	35.34	2.44	-5.72	0.67	30.60	8277.48
5	2.00	21.18	0.94	-19.03	0.59	91.12	25285.51
5	0.45	15.53	2.40	-13.58	0.52	21.00	5732.89
5	1.81	23.40	1.07	-6.85	0.61	84.06	22975.85
5	1.60	23.91	1.25	-3.83	0.50	74.95	20355.31
5	1.90	24.75	1.15	-8.69	0.65	88.39	24184.86
5	1.97	23.95	0.89	-4.72	0.62	92.26	25369.41
5	0.79	29.75	1.84	2.84	0.67	37.48	10196.17
5	0.20	28.43	2.05	-6.39	0.58	9.76	2611.10
5	1.97	23.94	0.89	-4.72	0.50	93.53	25721.77
5	0.90	23.94	1.03	-10.97	0.50	43.49	11791.57
5	1.87	24.18	0.80	-6.80	0.65	89.14	24555.48
5	0.55	21.74	2.31	-2.38	0.65	26.90	7237.87
5	1.60	25.17	1.25	-3.83	0.52	77.91	21178.71
5	1.96	20.75	0.86	-5.84	0.50	94.71	26007.49
5	0.50	23.08	0.96	6.68	0.50	24.34	6655.58
5	2.00	22.80	0.80	-6.40	0.57	97.58	26893.41
5	1.96	26.05	0.80	-15.83	0.65	95.31	26351.25
5	1.99	24.18	0.80	-6.80	0.65	98.42	27157.20
5	1.82	22.49	0.95	-3.56	0.70	90.74	24872.06
5	1.94	29.60	0.80	-15.84	0.72	99.77	27790.96
5	1.95	31.30	0.80	-14.77	0.70	100.73	28208.40
5	1.94	34.35	0.80	-15.96	0.50	101.35	28659.08
5	1.96	35.72	0.80	-11.71	0.50	101.94	29079.94
5	2.00	36.19	0.80	-15.99	0.60	103.83	29607.82
5	2.00	37.92	0.80	-4.76	0.54	103.98	29976.29
5	1.96	37.92	0.80	-15.97	0.50	102.42	29411.83
5	2.00	38.81	0.80	-15.99	0.61	105.10	30340.72
6	2.00	40.86	0.80	-15.98	0.60	105.86	30896.62

6	2.00	41.49	0.80	-14.97	0.62	106.05	31078.60
6	2.00	43.72	0.81	-15.97	0.50	106.93	31743.88
6	2.00	43.72	0.81	-15.97	0.52	106.93	31743.88
6	2.00	45.22	0.80	-15.98	0.50	107.75	32317.86
6	2.00	47.46	0.80	-15.98	0.50	109.07	33245.59
6	2.00	47.46	0.80	-15.98	0.51	109.07	33245.59
6	1.98	47.46	0.80	-15.98	0.50	107.92	32880.07

Table 6.3: The Pareto-front set of non-dominated solution set found by NSGA-II for parabolic design.

K	**H(m)**	$\beta(^0)$	**P(m)**	**E(m)**	$\psi(^0)$	Q(MWh)	Cost($)
2	0.20	36.43	1.54	0.62	96.03	2.66	927.73
2	0.20	42.04	1.65	0.67	93.37	2.66	927.73
2	1.33	33.80	1.80	0.62	98.45	19.22	6693.56
2	1.49	32.04	1.83	0.71	93.37	21.78	7584.68
2	1.62	30.30	1.89	0.67	93.37	24.04	8374.57
3	1.62	32.18	2.02	0.79	112.06	36.16	12594.96
3	1.31	36.44	1.89	0.56	73.55	28.45	9907.63
3	0.72	37.85	1.90	0.66	96.85	14.98	5217.01
3	1.25	36.85	1.95	0.68	105.28	26.85	9352.20
3	1.37	37.46	1.95	0.69	105.28	29.89	10410.81
3	1.37	25.69	2.05	0.54	84.72	29.79	10377.02
3	0.99	46.94	1.95	0.64	92.91	21.01	7319.14
4	1.36	40.49	1.94	0.67	105.28	39.33	13698.13
4	1.39	40.29	1.85	0.50	61.45	40.33	14047.05
4	0.59	27.82	2.12	0.56	75.28	16.19	5637.81
4	0.59	27.82	1.99	0.56	78.85	16.19	5637.81
4	0.74	46.94	1.95	0.66	117.70	20.38	7097.71
4	1.60	30.86	2.02	0.79	106.56	47.37	16498.91
4	1.75	22.77	2.25	0.86	96.49	52.35	18231.83
5	0.20	42.04	1.76	0.67	76.03	6.66	2319.32
5	0.93	42.56	2.01	0.57	104.15	32.44	11300.14
5	1.66	42.74	2.34	0.72	64.84	61.91	21563.11
5	1.46	42.56	1.94	0.61	74.31	52.89	18577.43
5	0.73	38.98	2.06	0.75	113.14	25.20	8777.03
5	1.17	42.56	2.01	0.57	83.78	41.67	14515.00
5	1.57	31.00	2.44	0.58	91.60	58.05	20217.74
5	1.91	23.30	2.24	0.63	103.32	72.71	25326.38
5	0.32	23.77	1.78	0.71	92.93	10.71	3729.97
5	1.49	37.18	1.96	0.69	111.89	54.75	19070.34
5	1.05	34.67	2.06	0.56	113.14	37.01	12889.87
5	1.63	24.27	2.44	0.64	87.05	60.42	21044.69
5	1.05	28.15	2.15	0.56	108.76	37.01	12889.87
5	1.49	37.18	1.96	0.71	96.49	54.75	19070.34
5	1.53	36.97	1.94	0.50	77.52	56.25	19591.63
5	1.53	35.03	1.94	0.50	77.52	56.25	19591.63
5	1.19	40.49	2.22	0.74	96.33	42.50	14802.01
6	1.95	26.44	2.24	0.57	103.67	89.21	31071.13
6	1.79	24.20	2.00	0.65	94.19	80.72	28114.58

6	2.00	26.44	2.24	0.58	107.14	91.99	32039.69
6	1.98	26.56	2.24	0.56	126.02	91.15	31746.71
6	1.18	39.95	1.97	0.57	92.69	50.49	17586.86
6	1.75	29.04	2.23	0.73	92.43	78.52	27347.75
6	1.37	42.56	1.89	0.56	85.11	59.56	20744.87
6	1.47	30.99	1.95	0.66	83.38	64.74	22547.94
6	0.30	26.44	2.22	0.58	111.03	12.01	4182.30
6	1.91	26.42	2.24	0.64	102.41	87.26	30391.66
6	0.20	25.41	1.95	0.66	97.77	7.99	2783.19
6	1.74	33.20	2.08	0.80	109.20	78.21	27246.20
6	1.07	15.97	2.07	0.58	106.89	45.64	15896.66
6	1.45	36.85	1.93	0.63	105.28	63.69	22182.01
6	1.91	26.42	2.24	0.64	103.32	87.26	30391.66
6	1.51	39.11	2.33	0.52	113.57	66.77	23256.65
6	1.65	38.07	2.07	0.56	96.33	73.14	25595.96
6	1.68	37.14	2.41	0.63	98.41	75.07	26146.54
6	1.84	25.41	2.02	0.71	95.93	83.04	29058.76
6	1.81	27.56	2.03	0.77	80.75	81.75	28580.68
6	1.51	39.11	2.31	0.52	121.84	66.77	23256.65
6	1.70	16.18	2.07	0.50	103.14	76.28	26568.21
6	1.82	27.56	2.03	0.77	87.07	82.04	28745.76
7	1.91	35.31	2.07	0.56	100.79	96.27	35497.29
7	1.81	31.97	2.02	0.63	83.75	93.12	33344.12
7	1.88	28.94	1.92	0.63	87.88	94.60	34746.87
7	1.94	32.76	2.04	0.61	90.57	97.85	36132.47
7	1.84	31.97	2.02	0.71	83.75	94.05	33901.88
7	2.00	32.76	2.04	0.51	93.59	99.93	37379.64
7	1.37	37.00	2.04	0.57	98.55	69.41	24176.82
7	1.37	35.02	2.04	0.57	98.55	69.41	24176.82
7	1.97	33.41	2.04	0.62	90.57	98.58	36767.80
7	1.65	38.07	2.07	0.58	96.33	85.32	29861.95
7	1.49	37.18	1.96	0.71	90.05	76.65	26698.47
7	1.99	42.39	2.26	0.58	90.57	98.84	37191.57
7	1.65	38.07	2.07	0.62	90.29	85.32	29861.95
7	1.30	33.18	1.96	0.54	105.04	65.78	22912.33
8	2.00	39.42	1.95	0.68	99.84	107.56	42719.59
8	1.86	32.97	1.76	0.57	87.74	100.67	39231.17
8	1.83	33.22	1.79	0.57	87.74	100.16	38428.87
8	1.98	39.12	1.92	0.69	108.34	106.13	42168.80
8	1.93	37.85	1.90	0.58	94.39	104.59	41062.74
8	1.96	39.42	1.92	0.50	99.84	105.08	41679.40
8	1.88	39.12	1.92	0.69	98.95	102.20	39710.71
8	1.92	39.42	1.92	0.53	88.47	103.35	40597.32
9	1.85	41.99	1.80	0.53	109.82	107.74	43811.81
9	1.96	41.56	1.80	0.53	111.62	113.09	47064.28
9	1.92	42.29	1.82	0.50	103.33	111.20	45879.64
9	1.95	38.85	1.74	0.55	98.34	112.35	46684.15
9	1.89	39.12	1.73	0.65	95.24	109.29	44872.26
9	1.99	38.79	1.73	0.53	100.69	114.12	47917.14
9	1.89	39.12	1.73	0.65	100.09	109.29	44872.26

9	2.00	43.97	1.88	0.54	113.80	115.13	48059.54
9	1.92	42.29	1.82	0.50	103.33	111.31	45949.64
10	2.00	47.53	1.83	0.52	118.41	122.71	53399.49
10	2.00	47.53	1.83	0.50	122.99	122.71	53399.49
10	1.90	46.34	1.77	0.58	94.39	117.22	50413.90
10	1.98	45.39	1.76	0.55	94.39	121.35	52863.86
10	1.86	45.95	1.76	0.54	85.11	115.21	49118.43
10	1.93	45.94	1.76	0.50	104.67	118.24	51148.53
10	1.97	45.40	1.76	0.55	102.65	120.53	52367.58
10	1.86	45.95	1.76	0.50	85.11	115.21	49118.43
10	1.95	45.94	1.76	0.50	104.67	119.34	51891.32
10	1.94	46.34	1.77	0.50	84.43	118.93	51563.81

As shown in Figure 6.3, two extreme points were pointed out. The first one of the end extreme points is having maximum cost and maximum absorbed energy) with (109.07 MWh/year, $33,245) and (122.71 MWh/year, $ 53,399) for the parabolic and flat designs, respectively. The second one can be the point with minimum cost and minimum absorbed energy with (2.66 MWh/year, $927) and (4.19 MWh/year, $1,118) for the parabolic and flat designs, respectively. From this, we can demonstrate that parabolic PV model was able to generate more energy after a point by the flat model cannot. On the other hand, the generated energy by the flat PV model was higher than the one generated by parabolic model for the same cost.

Also, Figure 6.3 shows the linear relationship between yearly collected energy and PV collector cost with these respective ranges (C = $[927; 32,039], Q = [2.66; 91.99] MWh/year) and (C = $[1,240; 27,157], Q = [4.64; 98.42] MWh/year) for parabolic and flat plates, respectively. Past, these ranges, their linear relationship have a higher slope (i.e. a large increasing of the cost with a small increasing of the absorbed energy for both designs). At the very beginning, both designs are absorbed almost the same energy with almost the same cost. After that, the flat model can harvest more energy with low cost compared to the parabolic model. However, after specific point (indicated by a red diamond), the parabolic model was still able to harvest energy whereas the flat model was not able to harvest more energy.

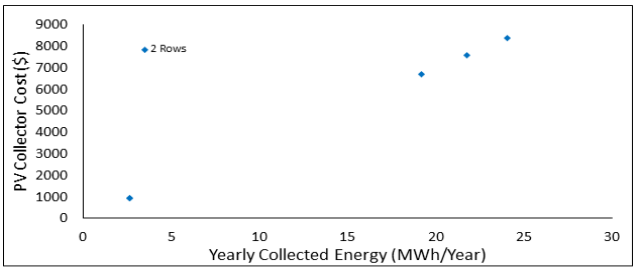

(a) 2 Rows

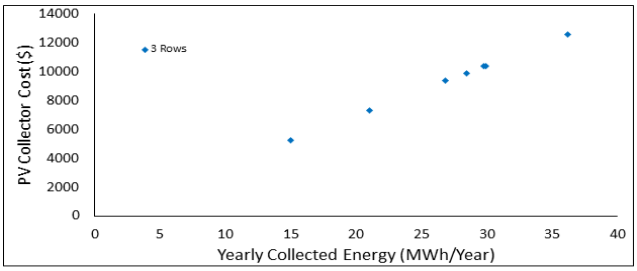

(b) 3 Rows

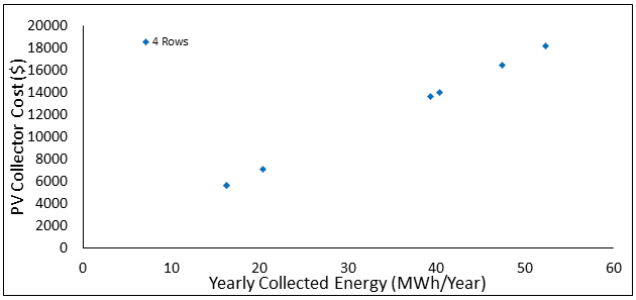

(c) 4 Rows

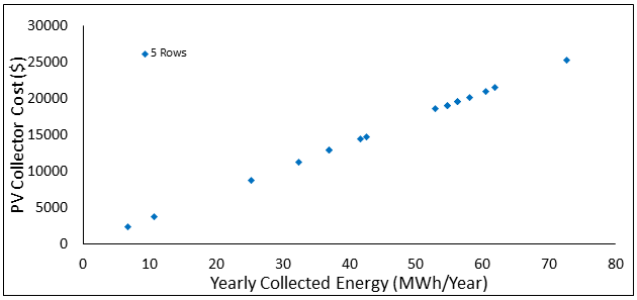

(d) 5 Rows

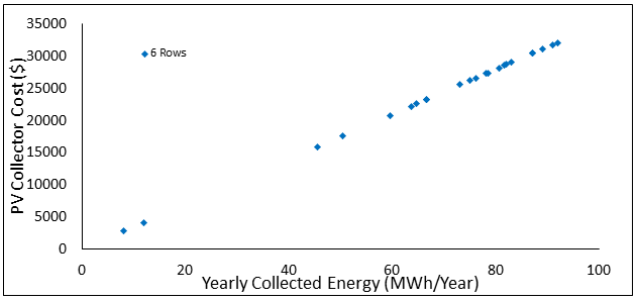

(e) 6 Rows

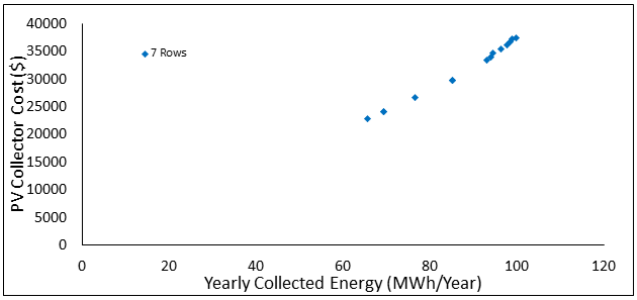

(f) 7 Rows

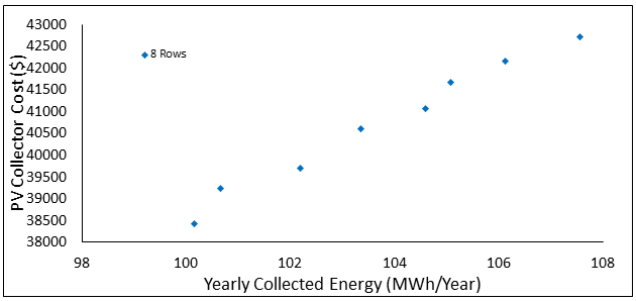

(g) 8 Rows

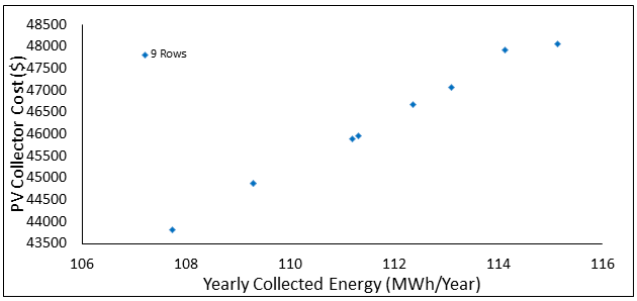

(h) 9 Rows

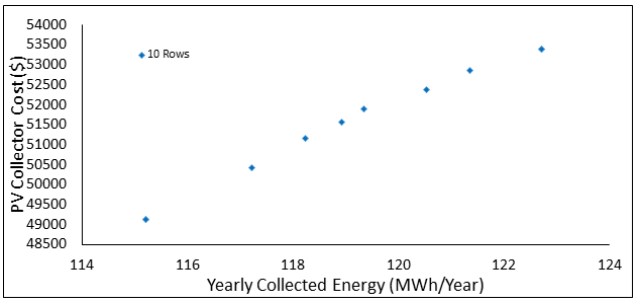

(i) 10 Rows

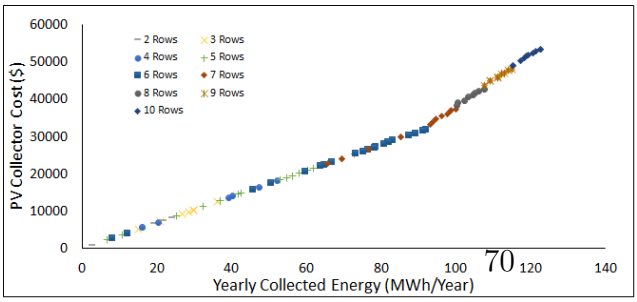

(j) All rows

Figure 6.1: The Pareto-front set of non-dominated solution set for parabolic plate found by NSGA-II with respect to number of collector rows.

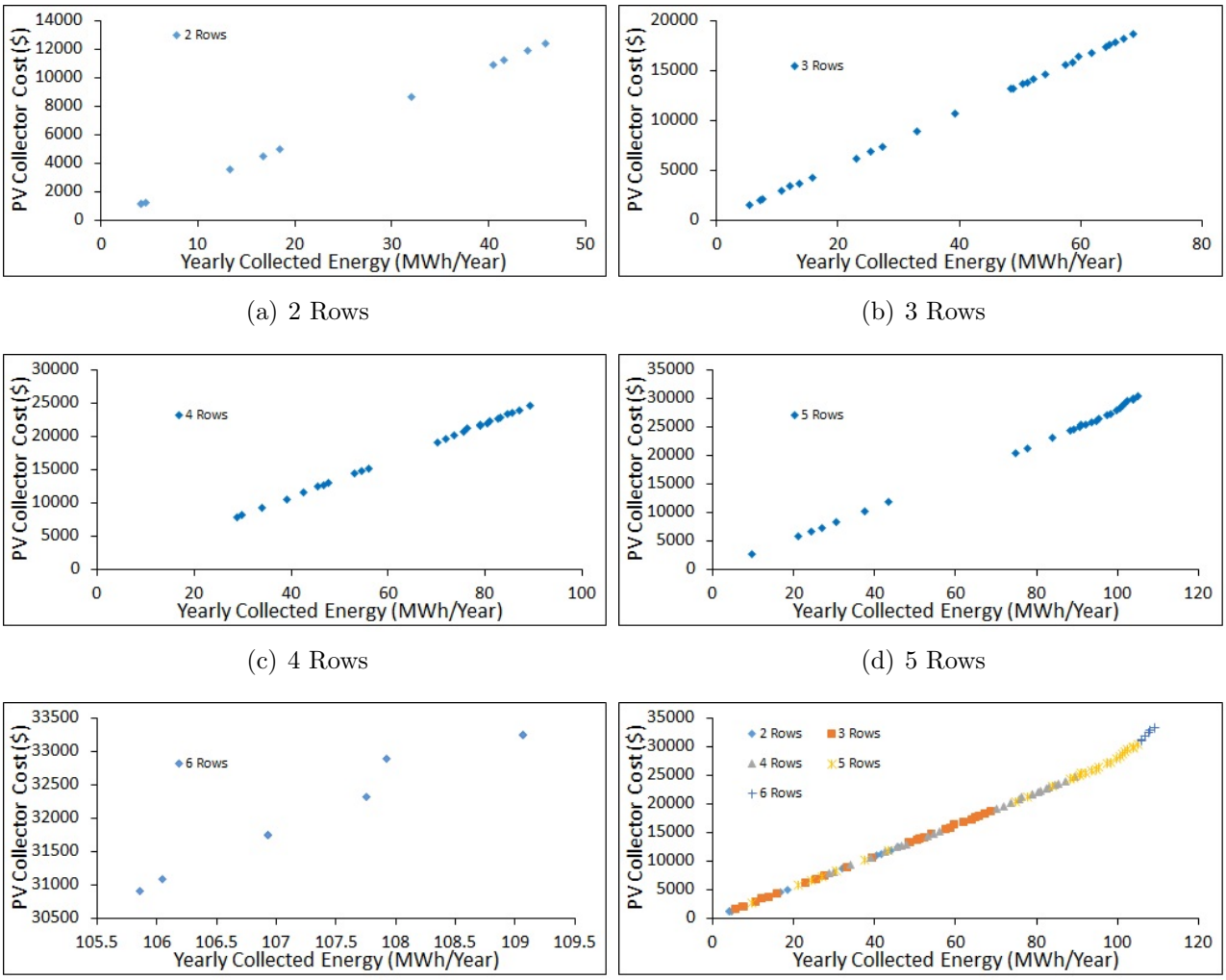

(a) 2 Rows (b) 3 Rows

(c) 4 Rows (d) 5 Rows

(e) 6 Rows (f) All rows

Figure 6.2: The Pareto-front set of non-dominated solutions for flat plate found by NSGA-II with respect to number of collector rows.

On the specific field width (W=12m, defined during the optimization), the flat design reached its maximum generated energy using six PVs (K=6). In this case, the number of used PVs will increase by increasing the width of the field. Because of the flat shape of these PVs it occupies more space than the parabolic one with the same dimensions (i.e., with same Height and length). By changing the maximum bounds of K to 100 with the same field parameters values (Width and Length), the same results were obtained for both designs. In other words, if we changed the bounds of K, we have to change the area of the

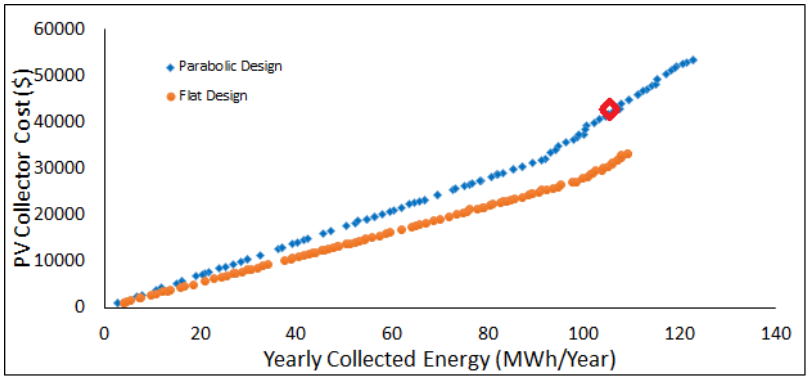

Figure 6.3: The Pareto-front set of non-dominated solutions for flat and parabolic designs found by NSGA-II.

land as well. In conclusion, the flat design still cannot reach to the maximum boundary of K even with a big value.

It can be seen, in Figures 6.1-j and 6.2-f, some solutions are overlapping. These solutions have the same objective functions values even with different decision variables, a decision maker can decide based on decision variables for the same objective values. His/her decision can be based on manufacturing factors, maintenance factors, etc. Also, there are some gaps in different locations of the Pareto front found by both design (Disconnected PF). This happened because of the discontinuity in the objective functions values (i.e., we do not have sequential values of the energy generated).

In Figure 6.1-h, two solutions have almost the same cost values with different energy generated values, which make these solutions at the same level on the graph. The opposite happened if Figure 6.2-e , one of the solutions with (K=6) seems out of the linearity of the graph. This is caused because of the small change in the energy value and big change in the cost compared with the other solutions.

When comparing the decision variables, for example, the collectors inclination angle (β), both designs could jump to the a higher inclination angles that satisfy problem constraints - from $\beta \approx 15$ to $\beta \approx 47$, which resulted with the highest energy Q = 109.07 MWh/year and 122.71 MWh/year for parabolic and flat plates, respectively. Moreover, the flat model reached its highest generated energy with $K = 6$; whereas the parabolic model

with $K = 10$ generated less energy than the flat one did.

As opposed to single objective optimization, when, we have just only one optimal solution, in multi-objective optimization, we have a set of optimal solutions. These solutions are trade-off solutions (Pareto solutions) because they are non-dominated solutions and its the decision maker's choice to select one of these solutions. For example, if an investor has sufficient amount of money and is looking into maximizing his ROI (return on investment), probably he will select the solution which obtained by the parabolic design (C = $ 53,399 and Q = 122.71 MWh/year). Other solutions with lower investment (e.g., C = $ 33,245 and Q = 109.07 MWh/year which obtained by the flat design) can also be selected if the investor has budget limitations by preserving the same ratio of ROI. In the case of having two solutions with the same output energy and cost, the decision variables will dramatically affect the decision making. For instance, the number of collectors (K) and the rim angle of the collector (ψ) have big impact on the manufacturing and transportation costs. Whereas, the field parameters, the center-to-center distance between collectors (P) and height of collectors above the ground (E), might affect the maintenance cost.

Chapter 7

Conclusions and Recommendations for Future Research

7.1 Conclusion

Converting the abundant flow of solar power to the Earth into affordable electricity is an enormous challenge. In other words, the goal is improving solar cell efficiency while holding down the cost per cell. PV modules currently in use are still limited to flat design. In this thesis, alternative cell and panel geometries have been proposed to harvest more energy over a typical day than a flat plate. Additionally, a comparison between the performance of these designs and flat PVs performance is presented. It is demonstrated that the proposed PV designs gain a small percentage in energy conversion efficiency, but the cost and complexity problems still exist in some designs. Besides, the power that they produce varies over the course of the day as the position of the Sun changes. Tracking PV systems are using to keep PV panels in an optimum position perpendicular to the solar radiation during the day time. As a result, the collected energy will increase. On the other hand, the power consumption by tracking device is 23% of the increased energy [58]. So, using tracking system for small-scale photovoltaic is not recommended. The use of PV tracking systems in large-scale applications like in farming, can be more useful. The optimum method of Sun tracking depends on the investment and the running cost. For instance, single-axis-tracking systems are quite cheaper and easier to implement, but their efficiency is lower than the two axes sun-tracking systems. In some cases, the PV arrays required to be fixed and maintained at a tilt angle. Finding the optimum tilt angle of PV panels depends mainly on the models used in calculations and the atmospheric environment of the location at which the experiments are conducted. By increasing the number of panels and height of these panels the total of the used land will increase; meanwhile, the shading area increases. As a result, the radiation energy received from the Sun will be reduced. To overcome all of these concerns, the optimal design of a solar field may be formulated mathematically as a constrained multi-objective optimization problem, and the solution maybe found by applying multi-objective optimization algorithms.

The main goal of the thesis is to seek optimum solar farm design in order to improve

the performance and reduce the cost. This thesis is considered the mathematical modeling of optimal solar farm design using parabolic trough collectors. Our objective is achieving maximum field incident energy with minimum cost. The solar collector field design formulated as an optimization problem. A multi-objective evolutionary algorithm (MOEA) called Non-dominated Sorting Genetic Algorithm-II (NSGI-II) is used to solve the modeled complex optimization problem. A comparison between using flat and parabolic trough panels in farm design is conducted. Numerical results are obtained at specific location (Toronto, Ontario), but can be obtained for any orientation and any latitude considering shading. Based on the achieved results, the maximum energy for the flat panels was Q = 109.07 MWh/year when the number of rows K = 6, the PV panel height H = 2 m, the PV inclination angle β =47.46^0, the distance between subsequent panels D = 80 cm, and the PV clearance above the ground E = 51 cm. Whereas, the maximum energy for the parabolic plate was Q = 122.71 MWh/year when the number of rows K = 10, the PV panel height H = 2 m, the PV inclination angle β = 47.53^0, the center to center distance between panels P = 1.83 m, and the PV clearance above the ground E = 50 cm.

As seen from the present results, there is a trade-off between the absolute values of the various objectives. and the solution will be selected based on the customer requirements and desires.

7.2 Recommendations for Future Research

Optimuzing the design of solar farm is a demanding topic. Some recommendations for future works can be summarized as follows:

1. Extending our work to combine reflectors with parabolic trough panels in order to harvest more light beams from the modules.

2. Extending the deployment of solar panels with tracking capability.

3. Utilizing flat and parabolic shapes together in the farm can be investigated.

4. Considering the maintenance and land costs.

5. Since, our work was as a first attempt to use solar panel with the parabolic trough shape, the mathematical modeling to consider the diffuse radiation was not available. The effects of the diffuse radiation should be taken into consideration later.

Bibliography

[1] A. Scheydecker, A. Goetzberger, and V. Wittver, "Reduction of reflection losses of pv modules by structured surfaces," in *Solar Energy*, 1994, pp. 171–176.

[2] P. J. Snchez-Illescas, P. Carpena, P. Bernaola-Galvn, M. Sidrach-De-Cardona, A. V. Coronado, and J. L. lvarez, "An analysis of geometrical shapes for pv module glass encapsulation," in *Solar Energy Materials and Solar Cells*, 2008, pp. 323–331.

[3] B. Myers, M. Bernardi, and J. C. Grossman, "Three-dimensional photovoltaic," in *Applied Physics Letters*, February 2010, pp. 1–8.

[4] M. Bernardi, N. Ferralis, J. H. Wan, R. Villalonc, and J. C. Grossman, "Solar energy generation in three dimensions," *Energy and Environmental Science*, pp. 6880–6884, 2012.

[5] A. Karavadi and R. S. Balog, "Novel non-flat photovoltaic module geometries and implications to power conversion," in *IEEE Energy Conversion Congress and Exposition (ECCE), 2011*, Sept 2011, pp. 7–13.

[6] V. Sugathan, N. Varma, E. John, and K. Sudhakar, "Design, development and testing of a novel triangular prism shaped solar cell," in *2013 International Conference on Green Computing, Communication and Conservation of Energy (ICGCE)*, Dec 2013, pp. 630–634.

[7] J. Liu, T. Luo, S. Mouli, F. Meng, B. Sun, M. Li, and J. Liu, "A novel coral-like porous sno2 hollow architecture: biomimetic swallowing growth mechanism and enhanced pho-

tovoltaic property for dye-sensitized solar cell application," *Chem. Commun.*, vol. 46, pp. 472–474, 2010.

[8] Z. Tachan, S. Rhle, and A. Zaban, "Dye-sensitized solar tubes: A new solar cell design for efficient current collection and improved cell sealing," *Solar Energy Materials and Solar Cells*, vol. 94, pp. 317–322, 2010.

[9] Z. Ning, Q. Zhang, H. Pei, J. Luan, C. Lu, Y. Cui, and H. Tian, "Photovoltage improvement for dye-sensitized solar cells via cone-shaped structural design," *Journal of Physical Chemistry C*, vol. 113, no. 23, pp. 10 307–10 313, 2009.

[10] S. R. Wenham, S. Bowden, M. Dickinson, R. Largent, N. Shaw, C. B. Honsberg, M. Green, and P. Smith, "Low cost photovoltaic roof tile," *Solar Energy Materials and Solar Cells*, vol. 47, no. 23, pp. 325–337, 1997.

[11] T. Maruyama and S. Osako, "Wedge-shaped light concentrator using total internal reflection," *Solar Energy Materials and Solar Cells*, vol. 57, no. 23, pp. 75–83, 1999.

[12] M. D. Hughes, M. Christopher, D.-A. Borca-Tasciuc, D. Polanco, and D. Kaminski, "Performance comparison of wedge-shaped and planar luminescent solar concentrators," *Renewable Energy*, vol. 52, pp. 266–272, 2013.

[13] J. Liu, J. Pan, G. E. Georgiou, K. K. Chin, Z. Zheng, and J. Tan, "A novel concentrator design with pv junctions on the sides of a flat panel," in *Photovoltaic Specialists Conference (PVSC), 2009 34th IEEE*, June 2009, pp. 001 127–001 131.

[14] A.-J. N. Khalifa and S. S. Al-Mutawalli, "Effect of two-axis sun tracking on the performance of compound parabolic concentrators," *Energy Conversion and Management*, vol. 39, no. 10, pp. 1073–1079, 1998.

[15] K. S. Karimov, M. Saqib, P. Akhter, M. Ahmed, J. Chattha, and S. Yousafzai, "A simple photo-voltaic tracking system," *Solar energy materials and solar cells*, vol. 87, no. 1, pp. 49–59, 2005.

[16] V. Sharma, J. Nayak, and S. Kedare, "Shading and available energy in a parabolic trough concentrator field," *Solar Energy*, vol. 90, pp. 144–153, 2013.

[17] J. A. Duffie and W. A. Beckman, *Solar Engineering of thermal processes.* John Wiley and Son publication Inc., 2006.

[18] D. Weinstock and J. Appelbaum, "Optimal solar field design of stationary collectors," *ASME Journal of Solar Energy Engineering*, pp. 898–905, 2004.

[19] A. Ibrahim, F. Bourennani, S. Rahnamayan, and G. F. Naterer, "Optimal photovoltaic system design with multi-objective optimization," *International Journal of Applied Metaheuristic Computing (IJAMC)*, vol. 4, no. 4, pp. 63–89, Oct. 2013.

[20] S. S. Rao and Y. Hu, "Multi-objective optimal design of stationary flat-plate solar collectors under probabilistic uncertainty," *Journal of Mechanical Design*, vol. 132, no. 9, pp. 1–6, 2010.

[21] S. S. Rao, H.-G. Lee, and Y. Hu, "Optimal design of compound parabolic concentrator solar collector system," *Journal of Mechanical Design*, vol. 136, no. 9, pp. 1–10, 2014.

[22] E. A. Mohamed, "Design and testing of a solar parabolic concentrating collector." Renewable Energy and Power Quality Journal, 2013, pp. 1–8.

[23] M. Gnther, M. Joemann, and S. Csambor, "Parabolic trough technology," in *Advanced CSP Teaching Materials*, A. Guizani, D. Krger, and T. Hirsch, Eds., 2010, ch. 5, pp. 1–106.

[24] H. Gunerhan, A. Hepbasli, and U. Giresunlu, "Environmental impacts from the solar energy systems," *Energy Source*, pp. 131–138, 2009.

[25] T. Razykov, "Photovoltaic solar electricity: state of the art and future prospects," in *Sixth International Conference on Electrical Machines and Systems. ICEMS 2003*, Nov 2003, pp. 297–301.

[26] B.-J. Huang, Y.-C. Huang, G.-Y. Chen, P.-C. Hsu, and K. Li, "Improving solar {PV} system efficiency using one-axis 3-position sun tracking," *Energy Procedia*, vol. 33, no. 0, pp. 280 – 287, 2013, {PV} Asia Pacific Conference 2012.

[27] S. Knowledge, "Three generations of photovoltaics," 2009. [Online]. Available: http://solarknowledge.blogspot.ca/2009/01/three-generations-of-photovoltaics.html

[28] U. Blieske, T. Doege, P. Gayout, M. Neander, D. Neumann, and A. Prat, "Light-trapping in solar modules using extra-white textured glass," in *The Third World Conference on Photovoltaic Energy Conversion*, May 2003, pp. 188–191.

[29] P. Campbell, S. R. Wenham, and M. A. Green, "Light trapping and reflection control with tilted pyramids and grooves," in *Photovoltaic Specialists Conference, 1988, Conference Record of the Twentieth IEEE*, 1988, pp. 713–716.

[30] M. Bernardi, D. J. Perreault, V. Bulovic, J. C. Grossman, and N. Ferralis, "Three-dimensional photovoltaic apparatus and method," *U.S. Patent 097485*, Jan 2012.

[31] H. Hiraki, A. Hiraki, M. Maeda, and Y. Takahashi, "Unique features of cylindrical type solar-module contrasted with plane or conventional type ones," *Journal of Physics: Conference Series*, pp. 1–5, 2012.

[32] L. Yong, S. Hui, and D. Youjun, "A novel solar cell fabricated with spiral photoelectrode for capturing sunlight 3-dimensionally," *Science China Technological Sciences*, vol. 49, pp. 663–673, 2006.

[33] E. Talbi, *Metaheuristics From Design to Implementation.* John Wiley and Sons publication Inc., 2009.

[34] K. Deb, A. Pratap, S. Agarwal, and T. Meyarivan, "A fast and elitist multi-objective genetic algorithm: NSGA-II," *IEEE Transactions on Evolutionary Computation*, no. 2, pp. 182–197, 2002.

[35] M. El-Kassaby, "Monthly and daily optimum tilt angle for south facing solar collectors; theoretical model, experimental and empirical correlations," *Solar and Wind Technology*, vol. 5, no. 6, pp. 589–596, 1988.

[36] O. Asowata, J. Swart, and C. Pienaar, "Optimum tilt and orientation angles for photovoltaic panels in the vaal triangle," in *Power and Energy Engineering Conference (APPEEC), 2012 Asia-Pacific*, June 2009, pp. 1–5.

[37] J. Kaldellis and D. Zafirakis, "Experimental investigation of the optimum photovoltaic panels tilt angle during the summer period," *Energy*, pp. 305–314, 2012.

[38] A. Mraoui, M. Khelif, and B. Benyoucef, "Optimum tilt angle of a photovoltaic system: Case study of algiers and ghardaia," in *Renewable Energy Congress (IREC), 2014 5th International*, March 2014, pp. 1–6.

[39] A. Chandrakar and Y. Tiwari, "Optimization of solar power by varying tilt angle/slope," *International Journal of Emerging Technology and Advanced Engineering*, pp. 145–150, April 2013.

[40] Tracstar. (2015) Should you install a solar tracker? [Online]. Available: http://www.helmholz.us/smallpowersystems/

[41] T. Tudorache and L. Kreindler, "Design of a solar tracker system for pv power plants," *Acta Polytechnica Hungarica*, vol. 7, no. 1, pp. 23–39, 2010.

[42] G. Chicco, J. Schlabbach, and F. Spertino, "Performance of grid-connected photovoltaic systems in fixed and sun-tracking configurations," *Power Tech, 2007 IEEE Lausanne*, pp. 677–682, July 2007.

[43] O. Aliman, I. Daut, M. Isa, and M. R. Adzman, "Simplification of sun tracking mode to gain high concentration solar energy," *American Journal of Applied Sciences*, vol. 4, no. 3, pp. 171–175, 2007.

[44] M. M. Abu-Khader, O. O. Badran, and S. Abdallah, "Evaluating multi-axes sun-tracking system at different modes of operation in jordan," *Renewable and Sustainable Energy Reviews*, vol. 12, no. 3, pp. 864–873, 2008.

[45] D. Sheen. (2011, Oct.) Born-again ziontist' revolutionizing solar energy field. [Online]. Available: http://www.haaretz.com/weekend/anglo-file/born-again-ziontist-revolutionizing-solar-energy-field-1.388639

[46] F. Bourennani, R. Rizvi, and S. Rahnamayan, "Optimal photovoltaic solar power farm design using the differential evolution algorithms," in *International Conference on Clean Energy (ICCI10)*, 2010, pp. 1–8.

[47] M. Vasile and L. Summerer, "Multi-objective optimisation of integrated space-based and terrestrial solar energy systems," in *61st International Astronautical Congress, IAC 2010*, 2010, pp. 1–10.

[48] V. Garg and M. N. Murty, "EPIC: Efficient integration of partitional clustering algorithms for classification," *Simulated Evolution and Learning*, vol. 6457, pp. 706–710, 2010.

[49] A. Khalkhali, M. Sadafi, J. Rezapour, and H. Safikhani, "Pareto based multi-objective optimization of solar thermal energy storage using genetic algorithms," *Transactions of the Canadian Society for Mechanical Engineering*, vol. 34, pp. 463–474, 2010.

[50] K. Deb, F. Ruiz, M. Luque, R. Tewari, J. M. Cabello, and J. M. Cejudo, "On the sizing of a solar thermal electricity plant for multiple objectives using evolutionary optimization," *Applied Soft Computing*, vol. 12, no. 10, pp. 3300–3311, 2012.

[51] A. Kornelakis, "Multiobjective particle swarm optimization for the optimal design of photovoltaic grid-connected systems," *Solar Energy*, vol. 84, no. 12, pp. 2022–2033, 2010.

[52] B. Myers, M. Bernardi, and J. C. Grossman, "Three-dimensional photovoltaic," in *Applied Physics Letters*, 2010, pp. 1–8.

[53] H. Nasiraghdam and S. Jadid, "Optimal hybrid PV/WT/FC sizing and distribution system reconfiguration using multi-objective artificial bee colony (MOABC) algorithm," *Solar Energy*, pp. 3057–3071, 2012.

[54] D. Suchitra, R. Utthra, D. R. Jegatheesan, and B. Tushar, "Optimization of a PV-Diesel hybrid stand-alone system using multi-objective genetic algorithm," *International Journal of Emerging Research in Management &Technology*, pp. 68–76, May 2013.

[55] D. Weinstock and J. Appelbaum, "Optimization of solar photovoltaic fields," *ASME Journal of Solar Energy Engineering*, pp. 1–10, 2009.

[56] Z. Yi, Q. Zhong, L. Peng, G. Wenwen, L. Qiming1, and H. Jia1, "Calculating the optimum tilt angle for parabolic solar trough concentrator with the north-south tilt tracking mode," in *Digital Manufacturing and Automation (ICDMA), 2013 Fourth International Conference on*, 2013, pp. 329–334.

[57] (2012, Agu) Monthly averaged hourly solar angles relative to the horizon and solar azimuth angles due south in degrees. national climate data and information archive. [Online]. Available: http://climat.meteo.gc.ca/prodsservs/indexe.html

[58] H. Mousazadeh, A. Keyhani, A. Javadi, H. Mobli, K. Abrinia, and A. Sharifi, "A review of principle and sun-tracking methods for maximizing solar systems output," *Renewable and Sustainable Energy Reviews*, vol. 13, no. 8, pp. 1800–1818, 2009.

Appendices

Appendix A

Tables

Table A.1: Monthly averaged hourly direct normal beam irradiance: Latitude 43.45^0 / Longitude -79.25^0(kWh/m^2)

Time	Jan	Feb	Mar	Apr	May	Jun	Jul	Aug	Sep	Oct	Nov	Dec
0:00	0.00000	0.00000	0.00000	0.00000	0.00000	0.00000	0.00000	0.00000	0.00000	0.00000	0.00000	0.00000
1:00	0.00000	0.00000	0.00000	0.00000	0.00000	0.00000	0.00000	0.00000	0.00000	0.00000	0.00000	0.00000
2:00	0.00000	0.00000	0.00000	0.00000	0.00000	0.00000	0.00000	0.00000	0.00000	0.00000	0.00000	0.00000
3:00	0.00000	0.00000	0.00000	0.00000	0.00000	0.00000	0.00000	0.00000	0.00000	0.00000	0.00000	0.00000
4:00	0.00000	0.00000	0.00000	0.00000	0.00000	0.00000	0.00000	0.00000	0.00000	0.00000	0.00000	0.00000
5:00	0.00000	0.00000	0.00000	0.00468	0.14674	0.15828	0.14806	0.01531	0.00000	0.00000	0.00000	0.00000
6:00	0.00000	0.00000	0.01569	0.15769	0.33691	0.26257	0.31192	0.20882	0.13394	0.00184	0.00000	0.00000
7:00	0.00000	0.02340	0.22030	0.26344	0.41847	0.33983	0.37807	0.31130	0.35083	0.16336	0.01726	0.00000
8:00	0.09385	0.17079	0.34287	0.33270	0.48868	0.38956	0.44376	0.38127	0.40981	0.22181	0.05722	0.06591
9:00	0.17957	0.25688	0.37952	0.37446	0.46091	0.44680	0.48069	0.41037	0.45062	0.25702	0.10449	0.14357
10:00	0.26265	0.30352	0.35457	0.40533	0.44297	0.44672	0.50614	0.41170	0.44010	0.33200	0.17526	0.22427
11:00	0.30753	0.32768	0.32872	0.43038	0.43691	0.45308	0.53128	0.39103	0.41262	0.33118	0.18037	0.24435
12:00	0.31932	0.35002	0.36153	0.40935	0.41892	0.43981	0.51153	0.40444	0.43877	0.30339	0.21458	0.27184
13:00	0.31121	0.32908	0.30974	0.38292	0.36645	0.41080	0.44172	0.38206	0.45567	0.29026	0.20413	0.26712
14:00	0.27772	0.31391	0.28671	0.33730	0.35479	0.36485	0.37597	0.36162	0.40584	0.30432	0.18164	0.18033
15:00	0.23116	0.31278	0.26168	0.34863	0.30725	0.33329	0.34918	0.34882	0.33139	0.26853	0.09025	0.11905
16:00	0.11487	0.25860	0.21181	0.30498	0.26215	0.31388	0.34373	0.32489	0.25700	0.17588	0.02441	0.00292
17:00	0.00000	0.05648	0.13422	0.22823	0.18940	0.27534	0.28033	0.24276	0.15046	0.01389	0.00000	0.00000
18:00	0.00000	0.00000	0.00000	0.06100	0.09217	0.19344	0.20778	0.13993	0.01434	0.00000	0.00000	0.00000
19:00	0.00000	0.00000	0.00000	0.00000	0.00548	0.09026	0.07403	0.00159	0.00000	0.00000	0.00000	0.00000
20:00	0.00000	0.00000	0.00000	0.00000	0.00000	0.00000	0.00000	0.00000	0.00000	0.00000	0.00000	0.00000
21:00	0.00000	0.00000	0.00000	0.00000	0.00000	0.00000	0.00000	0.00000	0.00000	0.00000	0.00000	0.00000
22:00	0.00000	0.00000	0.00000	0.00000	0.00000	0.00000	0.00000	0.00000	0.00000	0.00000	0.00000	0.00000
23:00	0.00000	0.00000	0.00000	0.00000	0.00000	0.00000	0.00000	0.00000	0.00000	0.00000	0.00000	0.00000

Appendix B

Permission Forms

License Number	3607350285141
License date	Apr 13, 2015
Licensed content publisher	Elsevier
Licensed content publication	Solar Energy
Licensed content title	Shading and available energy in a parabolic trough concentrator field
Licensed content author	None
Licensed content date	April 2013
Licensed content volume number	90
Licensed content issue number	n/a
Number of pages	10
Type of Use	reuse in a thesis/dissertation
Portion	full article
Format	electronic
Are you the author of this Elsevier article?	No
Will you be translating?	No
Title of your thesis/dissertation	Optimal Design of Parabolic Trough Solar Photovoltiac Farm Using Multi-objective Optimization
Expected completion date	Apr 2015
Estimated size (number of pages)	98
Elsevier VAT number	GB 494 6272 12
Permissions price	0.00 USD
VAT/Local Sales Tax	0.00 USD / 0.00 GBP
Total	0.00 USD

License Number	3607441434689
License date	Apr 14, 2015
Licensed content publisher	Elsevier
Licensed content publication	Solar Energy
Licensed content title	Reduction of reflection losses of PV-modules by structured surfaces
Licensed content author	A. Scheydecker,A. Goetzberger,V. Wittwer
Licensed content date	August 1994
Licensed content volume number	53
Licensed content issue number	2
Number of pages	6
Type of Use	reuse in a thesis/dissertation
Portion	figures/tables/illustrations
Number of figures/tables /illustrations	1
Format	both print and electronic
Are you the author of this Elsevier article?	No
Will you be translating?	No
Title of your thesis/dissertation	Optimal Design of Parabolic Trough Solar Photovoltiac Farm Using Multi-objective Optimization
Expected completion date	Apr 2015
Estimated size (number of pages)	98
Elsevier VAT number	GB 494 6272 12
Permissions price	0.00 USD
VAT/Local Sales Tax	0.00 USD / 0.00 GBP
Total	0.00 USD

Licensed content publisher	Elsevier
Licensed content publication	Solar Energy Materials and Solar Cells
Licensed content title	An analysis of geometrical shapes for PV module glass encapsulation
Licensed content author	None
Licensed content date	March 2008
Licensed content volume number	92
Licensed content issue number	3
Number of pages	9
Type of Use	reuse in a thesis/dissertation
Portion	figures/tables/illustrations
Number of figures/tables /illustrations	1
Format	both print and electronic
Are you the author of this Elsevier article?	No
Will you be translating?	No
Title of your thesis/dissertation	Optimal Design of Parabolic Trough Solar Photovoltiac Farm Using Multi-objective Optimization
Expected completion date	Apr 2015
Estimated size (number of pages)	98
Elsevier VAT number	GB 494 6272 12
Permissions price	0.00 USD
VAT/Local Sales Tax	0.00 USD / 0.00 GBP
Total	0.00 USD

License Number	3607450516197
Order Date	Apr 14, 2015
Publisher	AIP Publishing LLC
Publication	Applied Physics Letters
Article Title	Three-dimensional photovoltaics
Author	Bryan Myers,Marco Bernardi,Jeffrey C. Grossman
Online Publication Date	Feb 16, 2010
Volume number	96
Issue number	7
Type of Use	Thesis/Dissertation
Requestor type	Student
Format	Print and electronic
Portion	Figure/Table
Number of figures/tables	3
Title of your thesis / dissertation	Optimal Design of Parabolic Trough Solar Photovoltiac Farm Using Multi-objective Optimization
Expected completion date	Apr 2015
Estimated size (number of pages)	98
Total	0.00 USD

License Number	3607451069127
License date	Apr 14, 2015
Licensed content publisher	Royal Society of Chemistry
Licensed content publication	Energy & Environmental Science
Licensed content title	Solar energy generation in three dimensions
Licensed content author	Marco Bernardi,Nicola Ferralis,Jin H. Wan,Rachelle Villalon,Jeffrey C. Grossman
Licensed content date	Mar 8, 2012
Volume number	5
Issue number	5
Type of Use	Thesis/Dissertation
Requestor type	academic/educational
Portion	figures/tables/images
Number of figures/tables/images	3
Distribution quantity	5
Format	print and electronic
Will you be translating?	no
Order reference number	None
Title of the thesis/dissertation	Optimal Design of Parabolic Trough Solar Photovoltiac Farm Using Multi-objective Optimization
Expected completion date	Apr 2015
Estimated size	98
Total	0.00 USD

License Number	3607460752434
License date	Apr 14, 2015
Licensed content publisher	Royal Society of Chemistry
Licensed content publication	Chemical Communications (Cambridge)
Licensed content title	A novel coral-like porous SnO2 hollow architecture: biomimetic swallowing growth mechanism and enhanced photovoltaic property for dye-sensitized solar cell application
Licensed content author	Jinyun Liu,Tao Luo,Sitaramanjaneya Mouli T,Fanli Meng,Bai Sun,Minqiang Li,Jinhuai Liu
Licensed content date	Nov 16, 2009
Volume number	46
Issue number	3
Type of Use	Thesis/Dissertation
Requestor type	academic/educational
Portion	figures/tables/images
Number of figures/tables/images	1
Distribution quantity	5
Format	print and electronic
Will you be translating?	no
Order reference number	None
Title of the thesis/dissertation	Optimal Design of Parabolic Trough Solar Photovoltiac Farm Using Multi-objective Optimization
Expected completion date	Apr 2015
Estimated size	98
Total	0.00 USD

License Number	3607461001819
License date	Apr 14, 2015
Licensed content publisher	Elsevier
Licensed content publication	Solar Energy Materials and Solar Cells
Licensed content title	Dye-sensitized solar tubes: A new solar cell design for efficient current collection and improved cell sealing
Licensed content author	Zion Tachan,Sven Rühle,Arie Zaban
Licensed content date	February 2010
Licensed content volume number	94
Licensed content issue number	2
Number of pages	6
Type of Use	reuse in a thesis/dissertation
Portion	figures/tables/illustrations
Number of figures/tables /illustrations	1
Format	both print and electronic
Are you the author of this Elsevier article?	No
Will you be translating?	No
Title of your thesis/dissertation	Optimal Design of Parabolic Trough Solar Photovoltiac Farm Using Multi-objective Optimization
Expected completion date	Apr 2015
Estimated size (number of pages)	98
Elsevier VAT number	GB 494 6272 12
Permissions price	0.00 USD
VAT/Local Sales Tax	0.00 USD / 0.00 GBP
Total	0.00 USD

License Number	3607470685548
License date	Apr 14, 2015
Licensed content publisher	Elsevier
Licensed content publication	Solar Energy Materials and Solar Cells
Licensed content title	Low cost photovoltaic roof tile
Licensed content author	S.R. Wenham,S. Bowden,M. Dickinson,R. Largent,N. Shaw,C.B. Honsberg,M.A. Green,P. Smith
Licensed content date	October 1997
Licensed content volume number	47
Licensed content issue number	1-4
Number of pages	13
Type of Use	reuse in a thesis/dissertation
Portion	figures/tables/illustrations
Number of figures/tables /illustrations	1
Format	both print and electronic
Are you the author of this Elsevier article?	No
Will you be translating?	No
Title of your thesis/dissertation	Optimal Design of Parabolic Trough Solar Photovoltiac Farm Using Multi-objective Optimization
Expected completion date	Apr 2015
Estimated size (number of pages)	98
Elsevier VAT number	GB 494 6272 12
Permissions price	0.00 USD
VAT/Local Sales Tax	0.00 USD / 0.00 GBP
Total	0.00 USD

License Number	3607780071507
License date	Apr 14, 2015
Licensed content publisher	Elsevier
Licensed content publication	Energy Conversion and Management
Licensed content title	Effect of two-axis sun tracking on the performance of compound parabolic concentrators
Licensed content author	Abdul-Jabbar N. Khalifa,Salman S. Al-Mutawalli
Licensed content date	July 1998
Licensed content volume number	39
Licensed content issue number	10
Number of pages	7
Type of Use	reuse in a thesis/dissertation
Portion	figures/tables/illustrations
Number of figures/tables /illustrations	1
Format	both print and electronic
Are you the author of this Elsevier article?	No
Will you be translating?	No
Title of your thesis/dissertation	Optimal Design of Parabolic Trough Solar Photovoltiac Farm Using Multi-objective Optimization
Expected completion date	Apr 2015
Estimated size (number of pages)	98
Elsevier VAT number	GB 494 6272 12
Permissions price	0.00 USD
VAT/Local Sales Tax	0.00 USD / 0.00 GBP
Total	0.00 USD

License Number	3610080794153
License date	Apr 15, 2015
Licensed content publisher	Elsevier
Licensed content publication	Solar Energy Materials and Solar Cells
Licensed content title	Wedge-shaped light concentrator using total internal reflection
Licensed content author	Toshiro Maruyama,Satoshi Osako
Licensed content date	22 February 1999
Licensed content volume number	57
Licensed content issue number	1
Number of pages	9
Type of Use	reuse in a thesis/dissertation
Portion	figures/tables/illustrations
Number of figures/tables /illustrations	1
Format	both print and electronic
Are you the author of this Elsevier article?	No
Will you be translating?	No
Title of your thesis/dissertation	Optimal Design of Parabolic Trough Solar Photovoltiac Farm Using Multi-objective Optimization
Expected completion date	Apr 2015
Estimated size (number of pages)	98
Elsevier VAT number	GB 494 6272 12
Permissions price	0.00 USD
VAT/Local Sales Tax	0.00 USD / 0.00 GBP
Total	0.00 USD

License Number	3610080988404
License date	Apr 15, 2015
Licensed content publisher	Elsevier
Licensed content publication	Renewable Energy
Licensed content title	Performance comparison of wedge-shaped and planar luminescent solar concentrators
Licensed content author	Michael D. Hughes,Christopher Maher,Diana-Andra Borca-Tasciuc,David Polanco,Deborah Kaminski
Licensed content date	April 2013
Licensed content volume number	52
Licensed content issue number	n/a
Number of pages	7
Type of Use	reuse in a thesis/dissertation
Portion	figures/tables/illustrations
Number of figures/tables /illustrations	1
Format	both print and electronic
Are you the author of this Elsevier article?	No
Will you be translating?	No
Title of your thesis/dissertation	Optimal Design of Parabolic Trough Solar Photovoltiac Farm Using Multi-objective Optimization
Expected completion date	Apr 2015
Estimated size (number of pages)	98
Elsevier VAT number	GB 494 6272 12
Permissions price	0.00 USD
VAT/Local Sales Tax	0.00 USD / 0.00 GBP
Total	0.00 USD

License Number	3610100135703
License date	Apr 15, 2015
Licensed content publisher	Elsevier
Licensed content publication	Solar Energy Materials and Solar Cells
Licensed content title	A simple photo-voltaic tracking system
Licensed content author	Karimov Kh.S., Saqib M.A., Akhter P., Ahmed M.M., Chattha J.A. and Yousafzai S.A.
Licensed content date	May 2005
Licensed content volume number	87
Licensed content issue number	1-4
Number of pages	11
Type of Use	reuse in a thesis/dissertation
Portion	figures/tables/illustrations
Number of figures/tables /illustrations	1
Format	both print and electronic
Are you the author of this Elsevier article?	No
Will you be translating?	No
Title of your thesis/dissertation	Optimal Design of Parabolic Trough Solar Photovoltiac Farm Using Multi-objective Optimization
Expected completion date	Apr 2015
Estimated size (number of pages)	98
Elsevier VAT number	GB 494 6272 12
Permissions price	0.00 USD
VAT/Local Sales Tax	0.00 USD / 0.00 GBP
Total	0.00 USD